iScience

CellPress

Article

HDAC2 Regulates Site-Specific Acetylation of MDM2 and Its Ubiquitination Signaling in Tumor Suppression

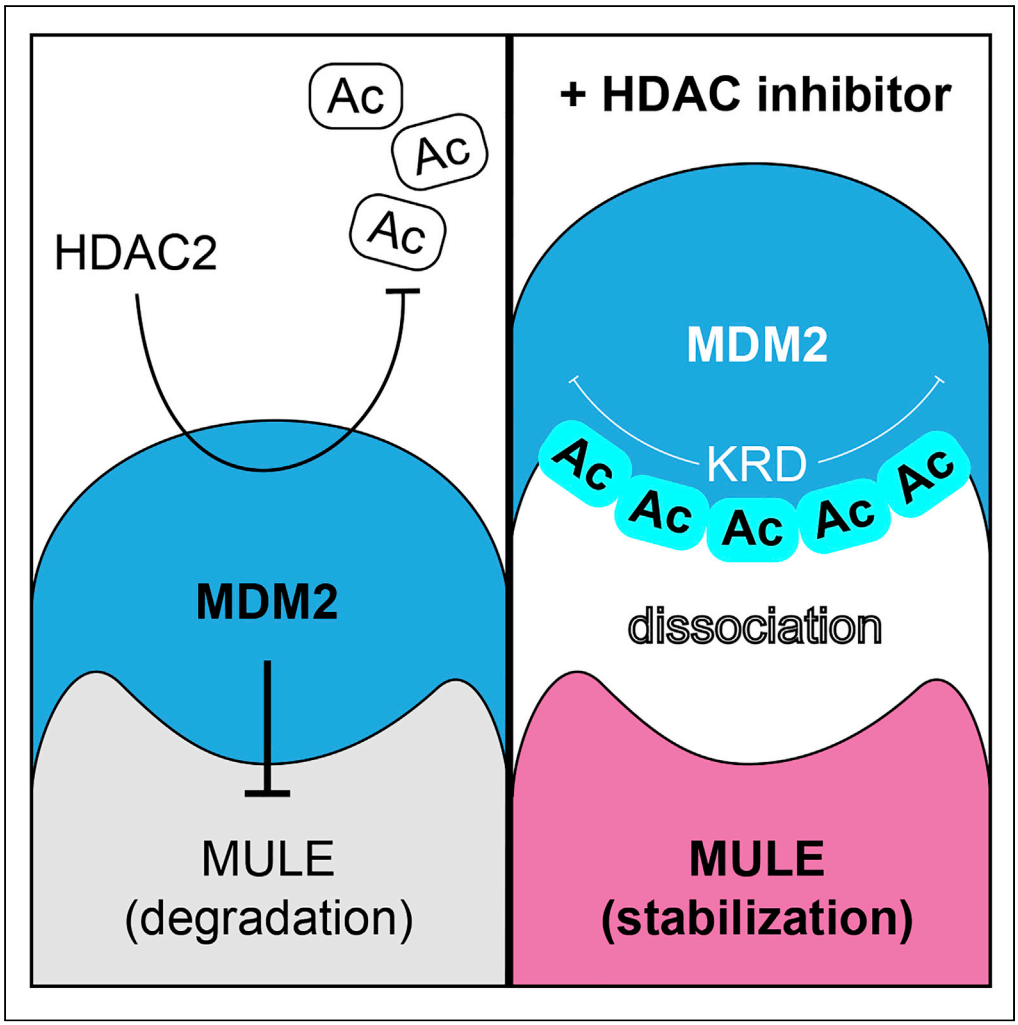

Nikita Patel, Juehong Wang, Kumiko Shiozawa, ..., Richard M. Myers, Tadashi Kondo, Le Su

lsu@hudsonalpha.org

HIGHLIGHTS

MULE undergoes MDM2/HDAC2-mediated degradation in synovial sarcoma

HDAC inhibition promotes MULE stabilization by acetylation and dissociation of MDM2

SS18-SSX fusion oncoprotein is a target of MULE E3 ligase

HDAC inhibitors downregulate SS18-SSX stability through the ubiquitin system

Patel et al., iScience 13, 43–54
March 29, 2019
https://doi.org/10.1016/j.isci.2019.02.008

iScience

CellPress

Article

HDAC2 Regulates Site-Specific Acetylation of MDM2 and Its Ubiquitination Signaling in Tumor Suppression

Nikita Patel,[1] Juehong Wang,[1,10] Kumiko Shiozawa,[2,10] Kevin B. Jones,[3,10] Yanfeng Zhang,[1] Jeremy W. Prokop,[1,4] George G. Davenport,[1] Naoe T. Nihira,[5] Zhenyue Hao,[6] Derek Wong,[7] Laurel Brandsmeier,[1] Sarah K. Meadows,[1] Arthur V. Sampaio,[7] Ryan Vander Werff,[7] Makoto Endo,[8] Mario R. Capecchi,[9] Kelly M. McNagny,[7] Tak W. Mak,[6] Torsten O. Nielsen,[8] T. Michael Underhill,[7,11] Richard M. Myers,[1,11] Tadashi Kondo,[2,11] and Le Su[1,11,12,*]

SUMMARY

Histone deacetylases (HDACs) are promising targets for cancer therapy, although their individual actions remain incompletely understood. Here, we identify a role for HDAC2 in the regulation of MDM2 acetylation at previously uncharacterized lysines. Upon inactivation of HDAC2, this acetylation creates a structural signal in the lysine-rich domain of MDM2 to prevent the recognition and degradation of its downstream substrate, MCL-1 ubiquitin ligase E3 (MULE). This mechanism further reveals a therapeutic connection between the MULE ubiquitin ligase function and tumor suppression. Specifically, we show that HDAC inhibitor treatment promotes the accumulation of MULE, which diminishes the t(X; 18) translocation-associated synovial sarcomagenesis by directly targeting the fusion product SS18-SSX for degradation. These results uncover a new HDAC2-dependent pathway that integrates reversible acetylation signaling to the anticancer ubiquitin response.

INTRODUCTION

Synovial sarcoma is an incurable malignant soft tissue tumor, which primarily affects children and young adults. Like many other sarcomas, this disease is histologically composed of mesenchymal cells. However, synovial sarcoma displays variable degrees of epithelial differentiation and contains a unique chromosomal translocation t(X; 18), which most commonly fuses the *SS18* gene with *SSX1* or *SSX2* (Nielsen et al., 2015). Depletion of SS18-SSX by small interfering RNAs (siRNAs) causes apoptotic cell death of human synovial sarcoma cells (Peng et al., 2008; Cai et al., 2011; Carmody Soni et al., 2014). Conversely, overexpression of SS18-SSX in noncancerous rat fibroblast cells shows transforming activity in a xenograft model (Nagai et al., 2001). Notably, mice conditionally expressing the SS18-SSX fusion gene in certain cell lineages develop tumors that are pathologically indistinguishable from and molecularly consistent with synovial sarcoma in humans (Haldar et al., 2007), thus confirming the critical role for SS18-SSX in the pathogenesis of synovial sarcoma.

Fundamental progress has been made in understanding how the SS18-SSX fusion protein promotes tumorigenesis, which indeed involves multiple parallel mechanisms, such as epigenetic remodeling (Su et al., 2012; Kadoch and Crabtree, 2013; Banito et al., 2018; McBride et al., 2018), cellular adhesion (Eid et al., 2000), mesenchymal-to-epithelial transition (Saito et al., 2006; Barrott et al., 2015), protein translocation (Pretto et al., 2006), and microRNA regulation (Hisaoka et al., 2011; Minami et al., 2014). Such complexities in SS18-SSX action make the development of targeted therapies for synovial sarcoma extremely challenging. Despite the lack of effective treatment options, several lines of evidence have shown that human synovial sarcoma cells are highly sensitive to histone deacetylase (HDAC) inhibitors in cell cultures and in a cell-line-based xenograft model (Ito et al., 2005; Laporte et al., 2017a). One well-supported explanation for the action of HDAC inhibitors is histone acetylation through which key tumor suppressor genes become epigenetically reactivated (Lubieniecka et al., 2008; Su et al., 2010, 2012; Laporte et al., 2017b). In the present study, we propose an additional, transcription-independent mechanism whereby HDAC inhibition facilitates proteasomal degradation of the SS18-SSX fusion protein. This action relies mostly on a novel combination of HDAC2 and MDM2 activities in concert with the MULE E3 ligase function. Our findings connect HDAC2 activity to oncogenic protein stabilization via a series of post-translational events, which constitute an acetylation-dependent ubiquitin pathway that may serve as a common therapeutic target in human cancers.

[1]HudsonAlpha Institute for Biotechnology, Huntsville, AL 35806, USA

[2]Division of Rare Cancer Research, National Cancer Center, Tokyo 104-0045, Japan

[3]Department of Orthopaedics and Huntsman Cancer Institute, University of Utah, Salt Lake City, UT 84112, USA

[4]Department of Pediatrics and Human Development, Michigan State University, Grand Rapids, MI 49503, USA

[5]Beth Israel Deaconess Medical Center, Harvard Medical School, Boston, MA 02115, USA

[6]Princess Margaret Cancer Centre, University of Toronto, Toronto, ON M5G 2C1, Canada

[7]Biomdical Research Centre, University of British Columbia, Vancouver, BC V6T 1Z3, Canada

[8]Genetic Pathology Evaluation Centre, Vancouver Coastal Health Research Institute, Vancouver, BC V5Z 1M9, Canada

[9]Department of Human Genetics, University of Utah, Salt Lake City, UT 84112, USA

[10]These authors contributed equally

[11]Senior author

[12]Lead Contact

*Correspondence: lsu@hudsonalpha.org

https://doi.org/10.1016/j.isci.2019.02.008

RESULTS

HDAC Inhibitor Treatment Reduces SS18-SSX Levels through the Ubiquitin System

To assess the *in vivo* efficacy of HDAC inhibition in synovial sarcoma, we generated transgenic mice expressing human *SS18-SSX2* fusion oncogene within the myogenic factor 5 (Myf5) lineage (Haldar et al., 2007). Treatment with the HDAC inhibitor FK228 on a weekly basis significantly reduced growth of mouse synovial sarcomas (Figures S1A and S1B), associated with remarkable cytoreductive activity (Figures S1C–S1H). In addition to the histological observations, we noticed that SS18-SSX2 protein abundance was substantially decreased in FK228-treated tumors (Figures 1A and 1B). Considering the fusion oncogene dependency in synovial sarcoma, we decided to examine the molecular mechanism of SS18-SSX downregulation upon HDAC inhibition. To this end, we first developed a CRISPR/Cas9-based genome editing approach for FLAG epitope tagging of endogenous SS18-SSX2 fusion oncoprotein in patient-derived SYO-1 cells (Figures S1I–S1K). Anti-FLAG western blots revealed that SS18-SSX levels remained constant through the early time points of FK228 treatment, but fell drastically after overnight stimulation (Figure S1L). Similar results were obtained in cells treated with other structurally different HDAC inhibitors, such as SB939 and PCI-24781 (Figure 1C). We also tested this in SS18-SSX1-associated synovial sarcoma cells (Yamato-SS) and found that treatment with the HDAC inhibitors FK228 and SB939 led to a marked reduction of SS18-SSX protein levels, coupled with impaired tumor cell growth (Figures 1D and 1E). Importantly, the mRNA levels of SS18-SSX remained unchanged (Figure S1M), whereas its protein stability was significantly reduced (Figures 1F and 1G). This effect was efficiently blocked by the proteasome inhibitor MG-132 (Figure 1C), and restoration of SS18-SSX levels correlated positively with increased conjugation of poly-ubiquitin chains (Figure 1H). Our findings indicate the existence of as-yet-undefined ubiquitin ligases that target SS18-SSX for proteasomal degradation.

MULE Ubiquitin Ligase Binds to SS18-SSX and Promotes Its Degradation

Next, we performed anti-FLAG immunoprecipitation to purify SS18-SSX-interacting proteins. Mass spectrometric analysis of the peptides uniquely enriched after HDAC inhibitor stimulation led to identification of MCL-1 ubiquitin ligase E3 (MULE), a HECT-type enzyme that plays a central role in the regulation of cell proliferation and tumorigenesis (Shmueli and Oren, 2005; Kao et al., 2018) (Figures 2A and 2B). Its interaction with the fusion oncoprotein was readily detected in both proximity ligation and immunoprecipitation assays (Figures 2C–2E). This binding event seemed to involve two fundamental domains in MULE, WWE and UBM, which co-occupied the repression domain (SSXRD) at the C-terminal end of SS18-SSX (Figures 3A–3D). Interestingly, there exists an alternatively spliced product of the SSX2 gene (dos Santos et al., 2000), containing a different C-terminal region (Figure S2A). We found that this variant failed to interact with MULE in SYO-1 cells, regardless of HDAC inhibitor stimulation (Figures S2B–S2D). Given the fact that MULE neither binds wild-type SS18 nor does its deletion affect SS18 protein expression (Figures S2E and S2F), we reasoned that the C-terminal SSXRD may play an indispensable role for SS18-SSX recognition by MULE E3 ligase.

We continued to assess whether SS18-SSX is a substrate of MULE, and found that *in vitro* synthesized fusion oncoprotein could be poly-ubiquitinated by cell extracts prepared from wild-type but not Mule-knockout mouse embryonic fibroblasts (Figures 4A–4C). Consistently, depletion of MULE by short hairpin RNA in SYO-1 cells prevented endogenous SS18-SSX ubiquitination upon HDAC inhibitor stimulation (Figure 4D). Removal of MULE-binding SSXRD domain strikingly reduced SS18-SSX ubiquitination levels (Figure 3E), suggesting that MULE ubiquitinates the fusion oncoprotein largely through their physical interaction. It should be noted that the SYT N-terminal Homolog (SNH) motif of SS18-SSX also contributed to MULE-mediated ubiquitination (Figure 3E). Given that the SNH-deleted (ΔSNH) mutant retained binding to MULE (Figure 3D), we reasoned that the critical SS18-SSX ubiquitination sites may be located within the SNH region. Indeed, previous studies have identified a lysine residue (K13) within wild-type SS18 protein that is ubiquitinated in human cell lines (Mertins et al., 2013; Udeshi et al., 2013). However, among four lysines, only mutating K23 to arginine (K23R) effectively blocked SS18-SSX ubiquitination (Figure 3E). Thus the mechanism underlying SS18-SSX ubiquitination likely differs from that for wild-type SS18. Together, these results provide molecular insights into MULE E3 ligase activity toward the fusion oncoprotein (Figure 3F).

To elucidate the biological significance of these findings, we examined the effect of the presence or absence of MULE on SS18-SSX protein expression upon HDAC inhibitor treatment. In SYO-1 cells,

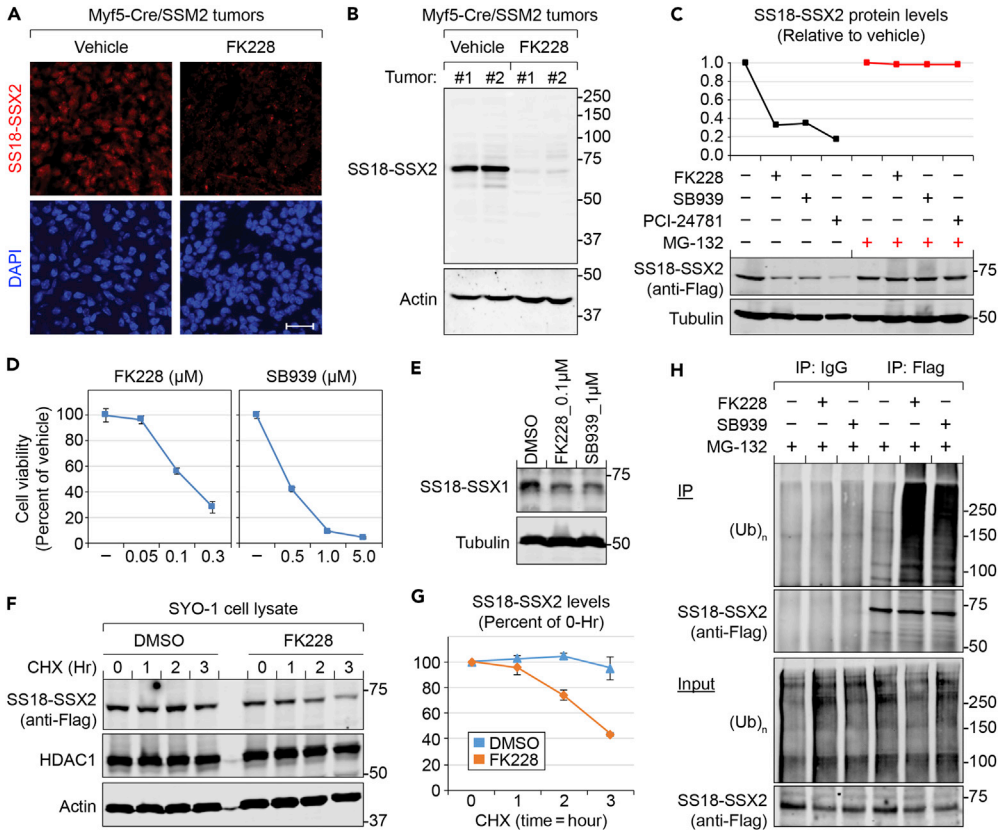

Figure 1. HDAC Inhibition Downregulates SS18-SSX Fusion Oncoprotein

(A) Representative immunofluorescence analysis of human SS18-SSX2 expression in tumor sections prepared from SSM2 mice treated with vehicle (–) or FK228 (3 mg/kg). Human SSX2 antibody was used to detect the fusion oncoprotein; DAPI was used for nuclear staining. Scale bar, 25 μm.

(B) Western blot analysis of human SS18-SSX2 expression in vehicle or FK228-treated SSM2 mouse tumors. Actin was used as a loading control.

(C) Western blot analysis of the lysate from CRISPR/Cas9-modified SYO-1 cells treated with vehicle (–) or HDAC inhibitors (FK228, SB939, and PCI-24781), in the presence and absence of MG-132. FLAG/tubulin ratios were normalized to vehicle and are shown in the top panel.

(D) Cell viability assay showing the sensitivity of Yamato-SS cells to FK228 and SB939 at different concentrations. Results represent mean ± SD of three independent experiments.

(E) Western blot analysis of SS18-SSX1 protein levels in DMSO-, FK228-, (100 nM), and SB939- (1 μM) treated Yamato-SS cell lysate. Tubulin was used as a loading control.

(F) Western blot analysis of SS18-SSX (anti-FLAG) protein abundance in CRISPR/Cas9-modified SYO-1 cells upon 12-h treatment of DMSO or FK228, followed by exposure to cycloheximide (CHX, 100 μg/mL) for the indicated time. Actin serves as a loading control, and HDAC1 serves as a negative control, which stays constant regardless of FK228 treatment.

(G) FLAG/actin ratios were normalized to the 0-h time point. Data represent mean ± SD of three independent experiments.

(H) Ubiquitination analysis of anti-FLAG immunoprecipitates from CRISPR-modified SYO-1 cells treated with DMSO, FK228, or SB939, in the presence of MG-132. Cell lysate (input) was applied to western blot analysis showing equal amounts of ubiquitin protein under all conditions, and mouse IgG was used as a negative control.

SS18-SSX levels fell after addition of FK228 and SB939. However, under the same conditions, the fusion oncoprotein avoided downregulation by MULE depletion (Figure 4E). More importantly, removal of MULE reduced the sensitivity of SYO-1 cells to HDAC inhibitors (Figures 4F and 4G). This resistance was neither due to the reported role of MULE in degrading histones (Liu et al., 2005) nor due to epigenetic changes in global histone acetylation upon HDAC inhibitor treatment (Figures S3A–S3C). This might result at least partly from impaired turnover of SS18-SSX, which retained the ability to promote cell proliferation and transformation via HDAC-independent mechanisms. In addition, among several known substrates of

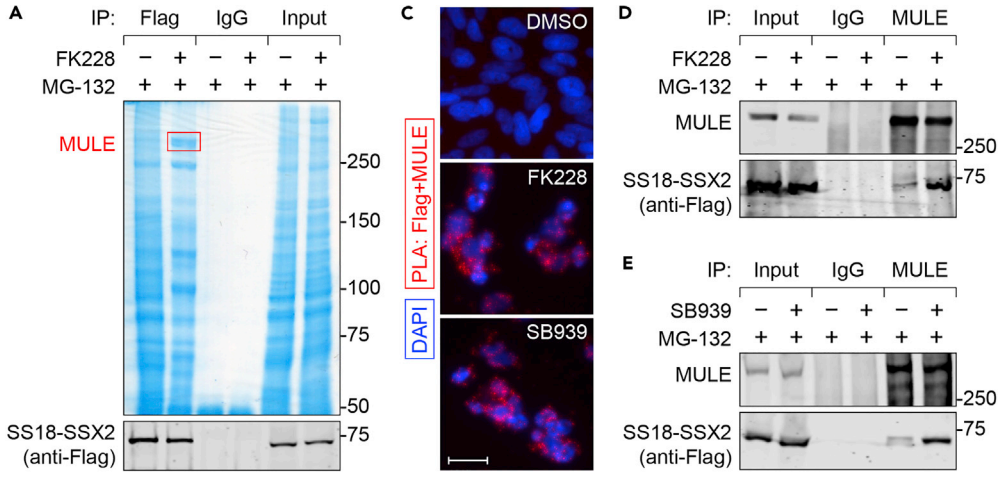

B

Query	Observed	Mr(expt)	Mr(calc)	ppm	Miss	Score	Expect	Rank	Unique	Peptide
211	350.6969	699.3792	699.3816	-3.50	0	36	0.012	1	U	K.FQIHR.D
358	835.4585	834.4513	834.4487	3.05	0	25	0.26	1	U	R.VLDFDVK.R
464	478.7339	955.4533	955.4545	-1.26	0	64	3.7e-005	1	U	K.EDMAVHVR.R
649	574.2538	1146.4931	1146.4975	-3.82	0	59	0.00014	1	U	R.AESPEEVACR.K
668	581.7744	1161.5343	1161.5349	-0.50	0	44	0.0044	1	U	R.NLCYHAQTR.H
807	657.2664	1312.5182	1311.5336	751	0	45	0.0028	1	U	K.ENGFGLAECCR.D
888	736.2958	1470.5771	1470.5789	-1.20	0	86	2.6e-007	1	U	R.DLSMSEEDQMMR.A
947	823.4040	1644.7935	1644.7963	-1.74	0	81	1.9e-006	1	U	R.AIAMSLGQDIPMDQR.A
999	948.9675	1895.9205	1895.9185	1.04	0	158	4.2e-014	1	U	R.SAATSGAGSTTSGVVSGSLGSR.E

Figure 2. MULE Binds to SS18-SSX upon HDAC Inhibitor Treatment

(A) Mass spectrometric analysis of anti-FLAG immunoprecipitates from CRISPR/Cas9-modified SYO-1 cells treated with DMSO or FK228. MULE was identified under the treatment of FK228; anti-FLAG western blot was performed to confirm the pull-down efficiency.

(B) List of the MULE peptides detected from anti-FLAG immunoprecipitates in FK228- (but not DMSO-) treated CRISPR/Cas9-modified SYO-1 cells.

(C) Proximity ligation assay for endogenous SS18-SSX (anti-FLAG) and MULE in CRISPR/Cas9-modified SYO-1 cells treated with DMSO, FK228, or SB939. DAPI was used to stain the nuclei; scale bar, 15 μm.

(D and E) MULE immunoprecipitation (IP) analysis of its interaction with the fusion oncoprotein (anti-FLAG) in DMSO-, FK228 (D)-, and SB939 (E)-treated CRISPR cells. The lysate (input) and rabbit IgG serve as positive and negative controls, respectively.

MULE, we found that HDAC inhibitor treatment downregulated CTCF and β-catenin protein expression, and this reduction was closely dependent on MULE (Figures S3D and S3E). CTCF is a multifunctional transcription factor that organizes chromatin architecture and controls genomic stability in various biological processes involved in tumorigenesis (Qi et al., 2012; Ghirlando and Felsenfeld, 2016; Song and Kim, 2017). β-Catenin acts as a central regulator of the WNT signaling pathway, which has been extensively studied in many human cancer types and directly linked to the progression of synovial sarcoma (Barham et al., 2013; Trautmann et al., 2014; Barrott et al., 2015, 2018; Cironi et al., 2016; Sanchez-Vega et al., 2018). Collectively, our findings point to MULE-mediated ubiquitination signaling as a potential fundamental target for HDAC inhibitors in tumor suppression.

HDAC Inhibition Stabilizes MULE by Acetylation and Dissociation of MDM2

We noted that MULE protein levels rose upon HDAC inhibitor treatment, without mRNA level changes (Figures S4A and S4B). Similar effects were also observed after proteasome inhibition (Figures 5A and S4C), indicating the unstable status of MULE protein in synovial sarcoma cells. Consistent with this notion, recent studies have reported MULE degradation by the oncogenic E3 ligase MDM2 in human cancers (Kurokawa et al., 2013; Canfield et al., 2016). We confirmed the endogenous interaction between MDM2 and MULE in both SYO-1 and Yamato-SS cells (Figures 5B and S4D). Knockdown of MDM2 by siRNAs led to increased levels of MULE, which inversely correlated with SS18-SSX downregulation and impaired cell viability (Figures 5C, 5D, S4E, and S4F). This effect seems independent of the p53 tumor suppressor, a key target of MDM2, because SYO-1 cells express wild-type p53, but Yamato-SS cells harbor a mutant p53 (R273C) (Vlenterie et al., 2016). Consistent with this view, depletion of endogenous p53 failed to rescue SYO-1 cells

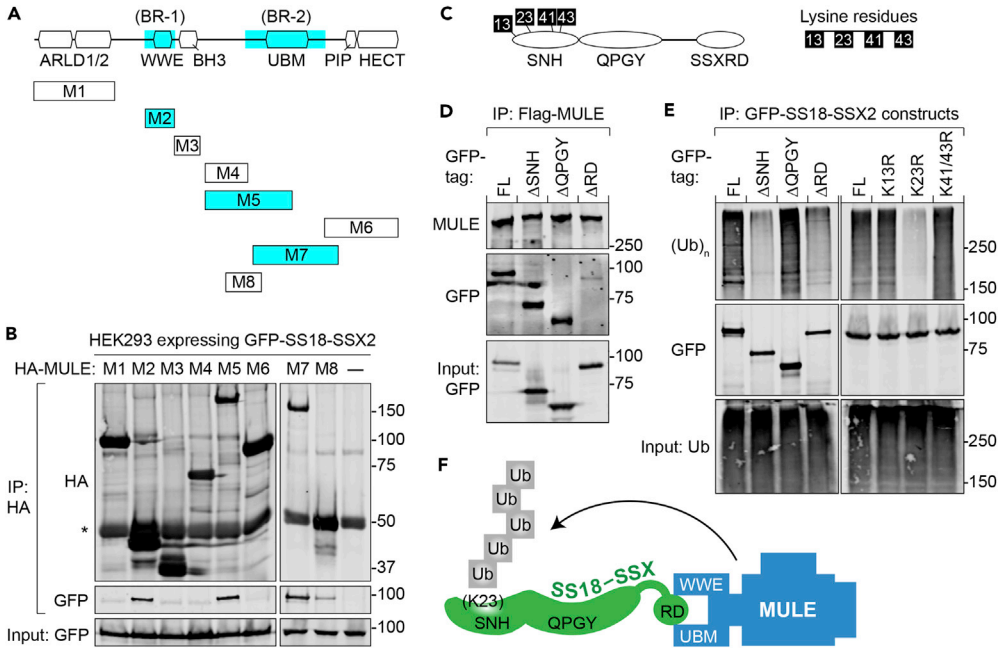

Figure 3. Molecular Mechanism of MULE-Mediated SS18-SSX Degradation

(A) Schematic of hemagglutinin (HA)-tagged MULE domains. ARLD, armadillo repeat-like domain; WWE, tryptophans-/glutamate-rich domain; BH3, BCL-2 homology 3 domain; UBM, ubiquitin-binding domain; PIP, PCNA-interacting protein domain; HECT, homologous to the E6-AP carboxyl terminus domain. BR indicates the SS18-SSX-binding region highlighted in blue.

(B) Anti-HA immunoprecipitation (IP) analysis of HEK293 cells expressing GFP-tagged SS18-SSX2, together with HA-tagged MULE constructs (or empty vector), under FK228 and MG-132 treatment. Cell lysate (input) serves as a positive control; *mouse IgG heavy chain.

(C) Schematic of GFP-tagged SS18-SSX2 construct. SNH, SYT N-terminal homolog domain; QPGY, glutamine-/proline-/glycine-/tyrosine-rich domain; SSXRD, SSX repression domain.

(D) Anti-FLAG immunoprecipitation analysis of HEK293 cells expressing full-length FLAG-MULE, together with GFP-SS18-SSX2 and its truncated mutants, under treatment with FK228 and MG-132. Cell lysate (input) was used as a positive control.

(E) Ubiquitination analysis of GFP-SS18-SSX2 and its mutants in FK228-treated HEK293 cells, in the presence of MG-132. Cell lysate (input) was applied to western blot analysis showing equal amounts of ubiquitin protein under all conditions.

(F) Model proposed for MULE-mediated SS18-SSX ubiquitination.

from MDM2 knockdown (Figures S4G–S4I). These results indicate a predominant role for MDM2 control of MULE (but not p53) signaling in synovial sarcoma cells. Notably, this action could be reversed by the addition of FK228 and SB939, which suppressed MDM2 binding to MULE (Figure 5E). As a result, HDAC inhibition led to a decrease in MULE ubiquitination and an increase in its protein stability (Figures 5F, 5G, S4J, and S4K). In addition, we found that the response of SYO-1 cells to FK228 and SB939 treatment, similar to MDM2 knockdown, remained unaffected after p53 deletion (Figures S4L–S4N), further supporting the notion that HDAC-inhibitor-induced anticancer action relies largely on MDM2 regulation of MULE, rather than p53, in synovial sarcoma.

Given that HDAC inhibition affects biological functions mostly through protein acetylation (Verdin and Ott, 2015), we investigated whether the same mechanism controls the MDM2-MULE interaction. Recently, it has been discovered that acetylation of the lysine-rich domain (KRD) can remove its positive charge and interrupt its association with the negatively charged acidic domain (Wang et al., 2016, 2017). Indeed, there does exist a lysine-rich stretch (amino acids 460–476) in the MDM2 protein, whereas MULE has an acidic domain between the residues 2425 and 2469. In support of these clues, we found structural evidence of MULE's acidic domain bound to the MDM2 KRD (Figures 6A, S5A, and S5B). This interaction likely involved five evolutionarily conserved lysine residues within KRD (Figures S5C–S5F), which were acetylated in endogenous and ectopically expressed MDM2 upon HDAC

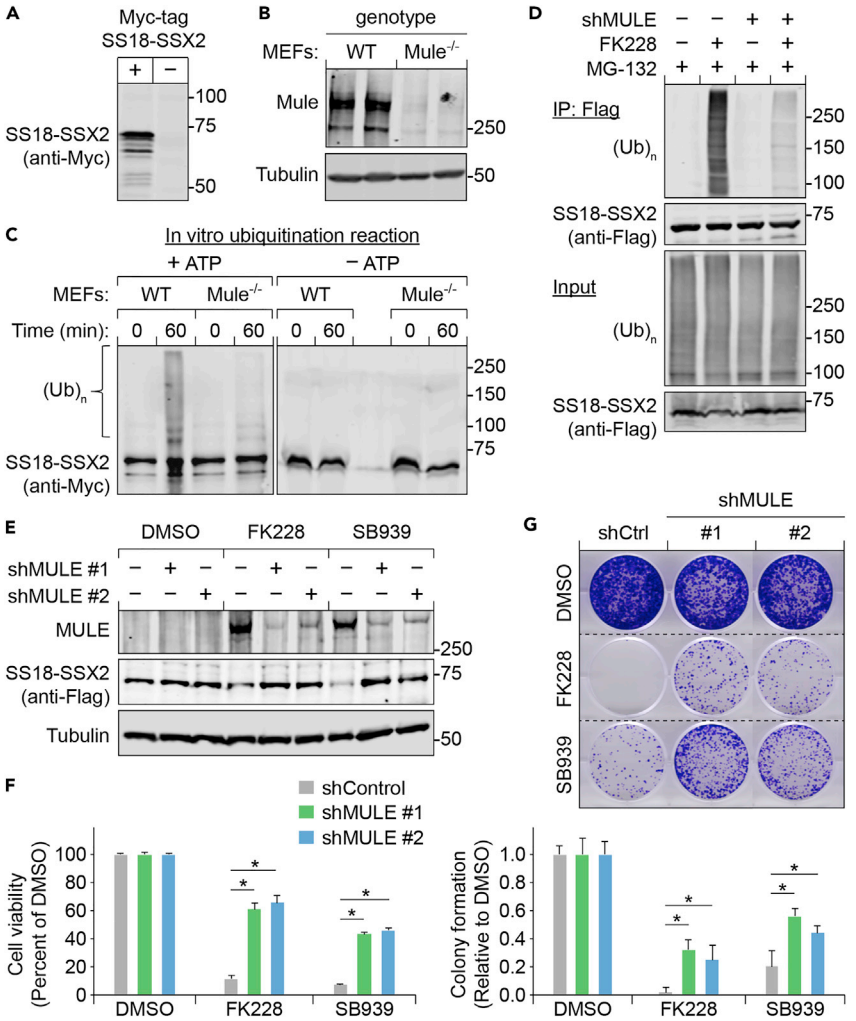

Figure 4. Knockdown of MULE Prevents SS18-SSX Downregulation and Promotes Resistance of Synovial Sarcoma Cells to HDAC Inhibition

(A) Anti-Myc western blot analysis of *in vitro* synthesized SS18-SSX2 protein. Empty vector (−) serves as a negative control.

(B) Wild-type (WT) and Mule-null mouse embryonic fibroblast (MEF) cells were subjected to western blots showing endogenous Mule protein levels. Tubulin was used as a loading control.

(C) Ubiquitin conjugation to Myc-tagged SS18-SSX2 protein after *in vitro* reactions supplemented with the indicated MEF cell extract. Reactions with no ATP serve as a negative control.

(D) SS18-SSX poly-ubiquitination in anti-FLAG immunoprecipitates prepared from control and MULE-knockdown CRISPR-modified SYO-1 cells treated with DMSO (−) or FK228 (30 nM), in the presence of the proteasome inhibitor MG-132. Input was applied to western blot analysis showing equal amounts of ubiquitin protein under all conditions.

(E) Western blot analysis of MULE and SS18-SSX (anti-FLAG) protein levels in CRISPR-modified SYO-1 cells stably expressing control or MULE short hairpin RNAs (shRNAs) upon treatment of DMSO and HDAC inhibitors (FK228 and SB939). Tubulin was used as a loading control.

(F) Viability assay of stable cell lines (used in E) in response to FK228 and SB939 treatment. Results represent mean ± SD of three independent experiments; *$p < 0.01$ by two-tailed Student's t test.

(G) Representative images of colony formation assay using DMSO-, FK228- and SB939-treated stable SYO-1 cell lines. Colony numbers under FK228 and SB939 treatment were normalized to vehicle (DMSO) and shown in the bottom panel. Data represent mean ± SD of three independent experiments; *$p < 0.01$ (two-tailed Student's t test).

inhibitor treatment (Figures 6B, 6C, S5G, and S5H). According to these properties, we generated a mutant MDM2 (5KR) in which all KRD lysine sites were replaced by arginine (Figure 6D). This acetylation-deficient mutation retained the ability of MDM2 binding to MULE, but exhibited resistance to HDAC-inhibitor-stimulated dissociation (Figure 6E). Point mutation analysis identified two acetylated

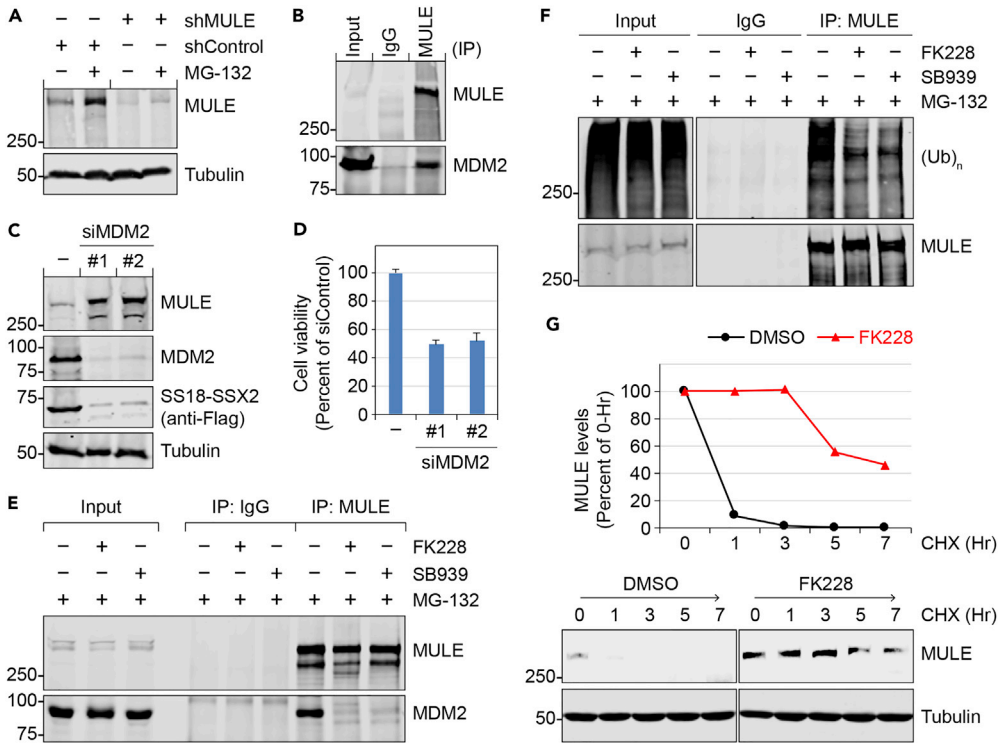

Figure 5. MDM2 Functions as a Negative Regulator of MULE

(A) Anti-MULE western blot analysis of the lysate prepared from SYO-1 cells treated with or without MG-132. MULE-depleted cell extracts were used as a negative control; tubulin serves as a loading control.

(B) Western blot analysis of anti-MULE immunoprecipitates from MG-132-treated SYO-1 cells. The lysate (input) and rabbit IgG serve as positive and negative controls, respectively.

(C) Western blot analysis of the lysate from CRISPR-modified SYO-1 cells transfected with control (–) or MDM2 siRNAs. Tubulin was used as a loading control.

(D) Viability of SYO-1 cells in response to MDM2 deletion by two individual siRNAs. Values were normalized to control knockdown (–); data represent mean ± SD of three independent experiments.

(E) Immunoprecipitation analysis of the MULE-MDM2 interaction in SYO-1 cells treated with DMSO (–) or HDAC inhibitors (FK228 and SB939), in the presence of MG-132. Cell lysate (input) and rabbit IgG serve as positive and negative controls, respectively.

(F) Ubiquitination analysis of endogenous MULE protein in vehicle (–), FK228- and SB939-treated SYO-1 cells. Cell lysate (input) was used to show equal amounts of ubiquitin under all conditions.

(G) Western blot analysis of MULE protein abundance in DMSO- and FK228-treated SYO-1 cells, upon exposure to cycloheximide (CHX) for the indicated time. Tubulin serves as a loading control, and MULE/tubulin ratios were normalized to the 0-h time point.

lysines, K469 and K470, responsible for the release of MDM2 from MULE (Figures 6F, 6G, S5I, and S5J). In line with this observation, K469 and K470 appeared to be the most effective sites of MDM2 acetylation after FK228 addition (Figure S5H). To further test this idea, we generated another MDM2 mutation in which the K469 and K470 residues were substituted to glutamine. This acetylation-mimicked mutation resulted in a dramatic loss of the MDM2-MULE interaction even without HDAC inhibitor treatment (Figures 6H and 6I). Intriguingly, Moshe Oren and colleagues reported that acetylation of the neighboring lysines K466 and K467 impairs MDM2's E3 ligase activity (Wang et al., 2004). However, a similar defect was not found when mimicking the acetylation of K469 and K470 (Figure S5K). Therefore different acetylation modifications in the KRD region might have distinct and cooperative roles in limiting MDM2 function.

HDAC2 Regulates the MDM2-MULE Interaction and Maintains SS18-SSX Protein Stability

Finally, it is important to determine which of the 11 HDAC family members act upstream of MDM2 (Figure S6A). We focused on two highly homologous members, HDAC1 and HDAC2, because they are

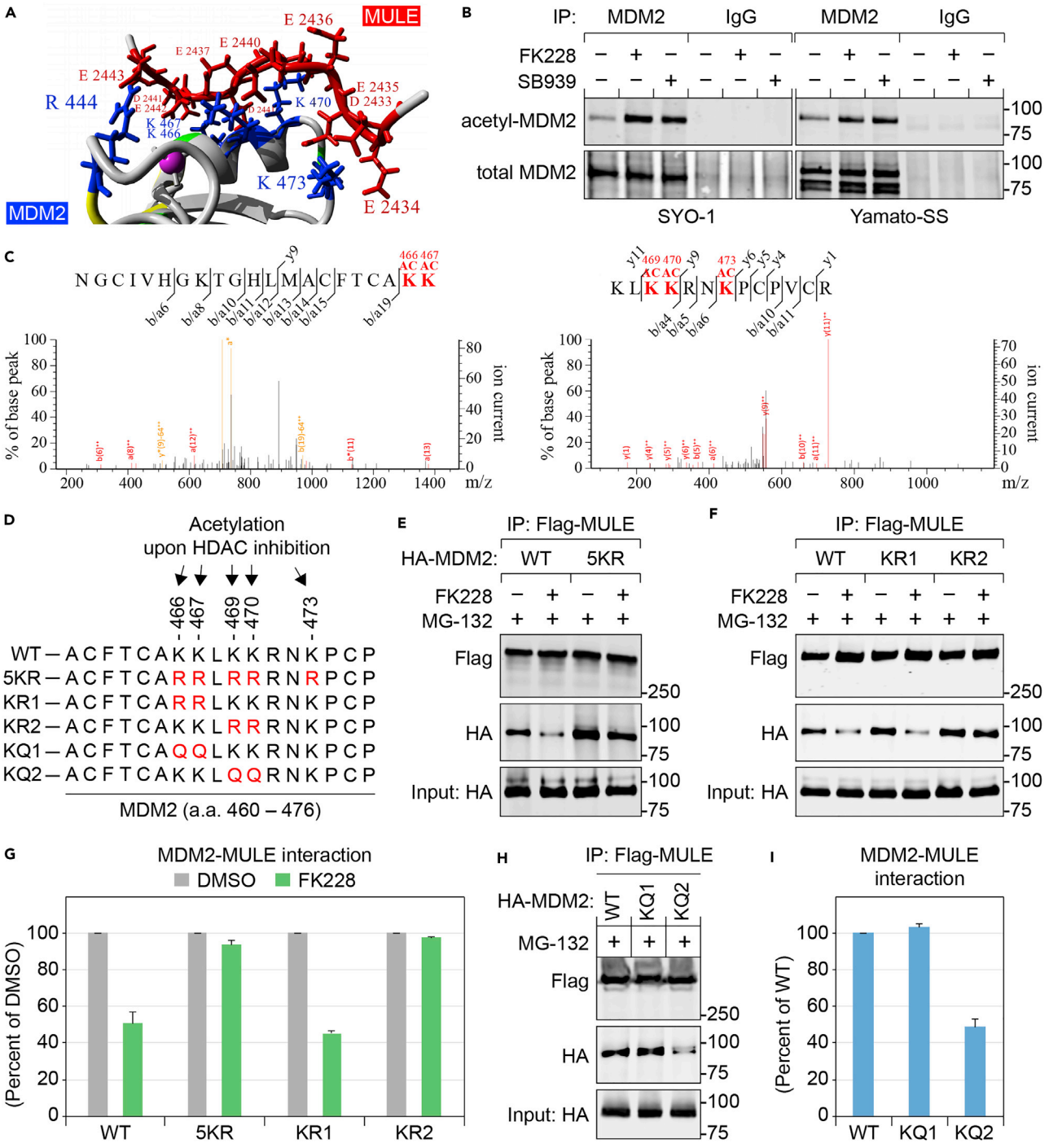

Figure 6. MDM2 Acetylation at Specific Lysine Sites Negatively Regulates its Interaction with MULE

(A) Structural interface showing the interaction between MDM2 (lysine-rich domain; KRD) and MULE (acidic domain).

(B) Acetyl-lysine western blots showing increased signals in endogenous MDM2 immunoprecipitates prepared from HDAC inhibitor (FK228/SB939)-treated SYO-1 and Yamato-SS cells, compared to DMSO (–). Rabbit IgG was used as a negative control.

(C) MS/MS spectra of the MDM2 lysine-rich domain (KRD) peptides identified in anti-MDM2 immunoprecipitates prepared from SYO-1 cells under the treatment of FK228, but not DMSO.

(D) Schematic of HA-tagged MDM2 (WT), acetylation-deficient (KR) and -mimicked (KQ) mutations.

(E) Immunoprecipitation analysis of MULE association with ectopically expressed MDM2 (WT) and its 5KR mutant in HEK293 cells treated with DMSO (–) or FK228, in the presence of MG-132. Input serves as a loading control.

Figure 6. *Continued*

(F) Immunoprecipitation analysis of MULE association with ectopically expressed MDM2 (WT) and its mutants (KR1 and KR2) in HEK293 cells treated with DMSO (–) or FK228, in the presence of MG-132. Input serves as a loading control.

(G) MULE-bound MDM2 levels were quantified by ImageJ and normalized to the Input; values of FK228-treated samples were further normalized to DMSO. Error bars represent mean ± SD of three independent experiments.

(H) Immunoprecipitation assay showing Flag-MULE interaction with HA-MDM2 and its KQ mutants in MG-132 treated HEK293 cells. The lysate (Input) was used as a loading control. (I) MULE-bound/input ratios of KQ mutants were normalized to WT. Results represent mean ± SD of three independent experiments.

most abundantly expressed in synovial sarcoma cells (Figure 7A) (Pacheco and Nielsen, 2012), and because the compound FK228 mainly inhibits HDAC1/2 activity. Interestingly, MDM2 associated with both HDAC1 and HDAC2 (Figure S6B), and depletion of neither HDAC1 nor HDAC2, affected MDM2 protein abundance (Figures S6C and S6D). However, MDM2-MULE interaction was diminished in HDAC2-deficient cells (Figures 7B and S6E). Moreover, the amount of SS18-SSX protein (but not mRNA) was drastically reduced upon HDAC2 knockdown (Figures 7C, S6F, and S6H), similar to the results obtained in MDM2-knockdown cells. We did not observe any significant effects after depletion of either HDAC1 or its Class I homolog HDAC3 (Figures S6G–S6I). Therefore unlike HDAC1, which contributes to SS18-SSX-mediated gene regulation (Su et al., 2012; Cironi et al., 2016), HDAC2 performs a nonredundant role in safeguarding the fusion oncoprotein from ubiquitin-mediated degradation.

DISCUSSION

The experiments presented here demonstrate a new mechanism for MDM2 inactivation, which is achieved through site-specific acetylation (Figure 7D). Repression of this acetylation is crucial to MDM2 interaction with its substrate MULE. In synovial sarcoma, the HDAC2 enzyme governs MDM2 substrate-binding activity; suppression of HDAC2 by RNA interference or small-molecule inhibitors allows dissociation and accumulation of the ubiquitin ligase MULE, leading to subsequent degradation of the SS18-SSX fusion oncoprotein, β-catenin, and CTCF. We provide mechanistic and functional evidence pointing toward the therapeutic implication for using HDAC inhibitors in synovial sarcoma treatment. Notably, this may not be limited to synovial sarcoma. For example, MDM2-mediated MULE downregulation has been reported to confer breast cancer resistance to the human epidermal growth factor receptor 2 inhibitor lapatinib (Kurokawa et al., 2013). It is tempting to speculate that use of HDAC inhibitors in combination therapy may resensitize some currently incurable cancers to conventional treatment.

Parallel with our current work, we recognize that MDM2 can also interact with MULE in an HDAC2-independent manner. This binding event requires the hydrophobic p53-binding pocket of MDM2, which in turn provides a targeting site for the small-molecule antagonist Nutlin-3a to prevent MULE accommodation and degradation (Kurokawa et al., 2013). In synovial sarcoma cells, however, Nutlin-3a treatment does not disrupt the MDM2-MULE complex, nor does it influence MULE protein expression (Figures S6J and S6K). These different results indicate that instead of a two-site binding model, there exist at least two levels of MDM2 control of MULE—one acting in the forward direction involving the intermolecular contact, whereas the second acting in the reverse direction involving lysine acetylation to unlock the binding interface. It will be important to further examine if any of the other post-translational modifications have a similar role as MDM2 in the regulation of MULE stability and activity. These efforts may also lead the way to a better understanding of how MDM2 integrates diverse input signals to execute its ubiquitination function with a high degree of specificity.

Limitations of the Study

We do not know if HDAC2 regulates MDM2 acetylation in any cancer forms other than synovial sarcoma. With our experiments, it is also not known if HDAC2 has a similar role in noncancerous context. Under different physiological conditions, HDAC2 and other related HDAC members may distinctly target the same lysine residues for control of MDM2 acetylation and function. Another limitation of our current study is the inability to answer whether HDAC inhibitors also control the substrate targeting of MULE E3 ligase through lysine acetylation. At this moment, the importance of post-translational modifications in the differential regulation of MULE downstream targets remains an open issue for further investigation.

METHODS

All methods can be found in the accompanying Transparent Methods supplemental file.

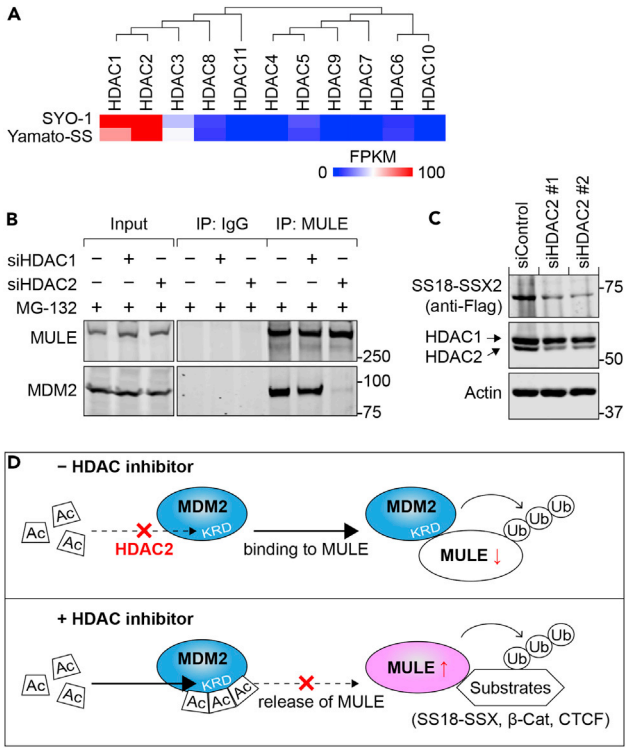

Figure 7. HDAC2 Contributes to MDM2-MULE Interaction and Governs SS18-SSX Protein Stability

(A) RNA sequencing analysis for the expression of HDAC family members in human synovial sarcoma cell lines, SYO-1 and Yamato-SS. FPKM, fragments per kilobase million.

(B) Immunoprecipitation analysis of the MDM2-MULE interaction in MG-132-treated SYO-1 cells depleted of HDAC1 or HDAC2. Cell lysate (input) and rabbit IgG serve as positive and negative controls, respectively.

(C) Western blot analysis of the lysate from nonspecific and HDAC2 knockdown CRISPR/Cas9-modified SYO-1 cells. Actin serves as a loading control.

(D) Proposed model for MDM2 control of MULE stability and activity through HDAC-inhibitor-induced lysine acetylation.

SUPPLEMENTAL INFORMATION

Supplemental Information includes Transparent Methods and six figures and can be found with this article online at https://doi.org/10.1016/j.isci.2019.02.008.

ACKNOWLEDGMENTS

We are grateful to Dr. Genze Shao (Peking University) and Dr. Qing Zhong (University of Texas Southwestern Medical Center) for providing human MULE plasmids. This work was supported by St. Baldrick's Foundation and HudsonAlpha Foundation (to L.S.), the Canadian Cancer Society Research Institute (to T.O.N. and T.M.U.), the National Institutes of Health (NIH) K08CA138764 (to K.B.J.), and NIH K01-ES025435 (to J.W.P.). K.B.J. also received additional support from the Damon Runyon Foundation and the Paul Nabil Bustany Fund for Synovial Sarcoma Research. The costs of animal care were partially covered by a one-time investigator-initiated grant from Celgene (to M.R.C.).

AUTHOR CONTRIBUTIONS

N.P., J.W., Y.Z., and G.G.D. designed and performed the experiments. K.S. and T.K. conducted mass spectrometry. K.B.J., Z.H., M.R.C., and T.W.M. carried out the animal studies. J.W.P. performed the structural analysis. N.T.N. assisted in characterizing MDM2-MULE interaction. D.W., A.V.S., R.V.W., M.E., K.M.M., T.O.N., and T.M.U. performed the experiments in the initial stage of this study. L.B., S.K.M., and R.M.M. guided CRISPR/Cas9 genome editing. L.S. supervised the study and wrote the manuscript with input from the other authors.

DECLARATION OF INTERESTS

The authors declare no competing interests.

Received: October 23, 2018
Revised: January 10, 2019
Accepted: February 11, 2019
Published: March 29, 2019

REFERENCES

Banito, A., Li, X., Laporte, A.N., Roe, J.S., Sanchez-Vega, F., Huang, C.H., Dancsok, A.R., Hatzi, K., Chen, C.C., Tschaharganeh, D.F., et al. (2018). The SS18-SSX oncoprotein hijacks KDM2B-PRC1.1 to drive synovial sarcoma. Cancer Cell *33*, 527–541.e8.

Barham, W., Frump, A.L., Sherrill, T.P., Garcia, C.B., Saito-Diaz, K., VanSaun, M.N., Fingleton, B., Gleaves, L., Orton, D., Capecchi, M.R., et al. (2013). Targeting the Wnt pathway in synovial sarcoma models. Cancer Discov. *3*, 1286–1301.

Barrott, J.J., Illum, B.E., Jin, H., Hedberg, M.L., Wang, Y., Grossmann, A., Haldar, M., Capecchi, M.R., and Jones, K.B. (2018). Paracrine osteoprotegerin and beta-catenin stabilization support synovial sarcomagenesis in periosteal cells. J. Clin. Invest. *128*, 207–218.

Barrott, J.J., Illum, B.E., Jin, H., Zhu, J.F., Mosbruger, T., Monument, M.J., Smith-Fry, K., Cable, M.G., Wang, Y., Grossmann, A.H., et al. (2015). beta-catenin stabilization enhances SS18-SSX2-driven synovial sarcomagenesis and blocks the mesenchymal to epithelial transition. Oncotarget *6*, 22758–22766.

Cai, W., Sun, Y., Wang, W., Han, C., Ouchida, M., Xia, W., Zhao, X., and Sun, B. (2011). The effect of SYT-SSX and extracellular signal-regulated kinase (ERK) on cell proliferation in synovial sarcoma. Pathol. Oncol. Res. *17*, 357–367.

Canfield, K., Wells, W., Geradts, J., Kinlaw, W.B., Cheng, C., and Kurokawa, M. (2016). Inverse association between MDM2 and HUWE1 protein expression levels in human breast cancer and liposarcoma. Int. J. Clin. Exp. Pathol. *9*, 6342–6349.

Carmody Soni, E.E., Schlottman, S., Erkizan, H.V., Uren, A., and Toretsky, J.A. (2014). Loss of SS18-SSX1 inhibits viability and induces apoptosis in synovial sarcoma. Clin. Orthop. Relat. Res. *472*, 874–882.

Cironi, L., Petricevic, T., Fernandes Vieira, V., Provero, P., Fusco, C., Cornaz, S., Fregni, G., Letovanec, I., Aguet, M., and Stamenkovic, I. (2016). The fusion protein SS18-SSX1 employs core Wnt pathway transcription factors to induce a partial Wnt signature in synovial sarcoma. Sci. Rep. *6*, 22113.

dos Santos, N.R., Torensma, R., de Vries, T.J., Schreurs, M.W., de Bruijn, D.R., Kater-Baats, E., Ruiter, D.J., Adema, G.J., van Muijen, G.N., and van Kessel, A.G. (2000). Heterogeneous expression of the SSX cancer/testis antigens in human melanoma lesions and cell lines. Cancer Res. *60*, 1654–1662.

Eid, J.E., Kung, A.L., Scully, R., and Livingston, D.M. (2000). p300 interacts with the nuclear proto-oncoprotein SYT as part of the active control of cell adhesion. Cell *102*, 839–848.

Ghirlando, R., and Felsenfeld, G. (2016). CTCF: making the right connections. Genes Dev. *30*, 881–891.

Haldar, M., Hancock, J.D., Coffin, C.M., Lessnick, S.L., and Capecchi, M.R. (2007). A conditional mouse model of synovial sarcoma: insights into a myogenic origin. Cancer Cell *11*, 375–388.

Hisaoka, M., Matsuyama, A., Nagao, Y., Luan, L., Kuroda, T., Akiyama, H., Kondo, S., and Hashimoto, H. (2011). Identification of altered MicroRNA expression patterns in synovial sarcoma. Genes Chromosomes Cancer *50*, 137–145.

Ito, T., Ouchida, M., Morimoto, Y., Yoshida, A., Jitsumori, Y., Ozaki, T., Sonobe, H., Inoue, H., and Shimizu, K. (2005). Significant growth suppression of synovial sarcomas by the histone deacetylase inhibitor FK228 in vitro and in vivo. Cancer Lett. *224*, 311–319.

Kadoch, C., and Crabtree, G.R. (2013). Reversible disruption of mSWI/SNF (BAF) complexes by the SS18-SSX oncogenic fusion in synovial sarcoma. Cell *153*, 71–85.

Kao, S.H., Wu, H.T., and Wu, K.J. (2018). Ubiquitination by HUWE1 in tumorigenesis and beyond. J. Biomed. Sci. *25*, 67.

Kurokawa, M., Kim, J., Geradts, J., Matsuura, K., Liu, L., Ran, X., Xia, W., Ribar, T.J., Henao, R., Dewhirst, M.W., et al. (2013). A network of substrates of the E3 ubiquitin ligases MDM2 and HUWE1 control apoptosis independently of p53. Sci. Signal. *6*, ra32.

Laporte, A.N., Barrott, J.J., Yao, R.J., Poulin, N.M., Brodin, B.A., Jones, K.B., Underhill, T.M., and Nielsen, T.O. (2017a). HDAC and proteasome inhibitors synergize to activate pro-apoptotic factors in synovial sarcoma. PLoS One *12*, e0169407.

Laporte, A.N., Poulin, N.M., Barrott, J.J., Wang, X.Q., Lorzadeh, A., Vander Werff, R., Jones, K.B., Underhill, T.M., and Nielsen, T.O. (2017b). Death by HDAC inhibition in synovial sarcoma cells. Mol. Cancer Ther. *16*, 2656–2667.

Liu, Z., Oughtred, R., and Wing, S.S. (2005). Characterization of E3Histone, a novel testis ubiquitin protein ligase which ubiquitinates histones. Mol. Cell. Biol. *25*, 2819–2831.

Lubieniecka, J.M., de Bruijn, D.R., Su, L., van Dijk, A.H., Subramanian, S., van de Rijn, M., Poulin, N., van Kessel, A.G., and Nielsen, T.O. (2008). Histone deacetylase inhibitors reverse SS18-SSX-mediated polycomb silencing of the tumor suppressor early growth response 1 in synovial sarcoma. Cancer Res. *68*, 4303–4310.

McBride, M.J., Pulice, J.L., Beird, H.C., Ingram, D.R., D'Avino, A.R., Shern, J.F., Charville, G.W., Hornick, J.L., Nakayama, R.T., Garcia-Rivera, E.M., et al. (2018). The SS18-SSX fusion oncoprotein hijacks BAF complex targeting and function to drive synovial sarcoma. Cancer Cell *33*, 1128–1141.e7.

Mertins, P., Qiao, J.W., Patel, J., Udeshi, N.D., Clauser, K.R., Mani, D.R., Burgess, M.W., Gillette, M.A., Jaffe, J.D., and Carr, S.A. (2013). Integrated proteomic analysis of post-translational modifications by serial enrichment. Nat. Methods *10*, 634–637.

Minami, Y., Kohsaka, S., Tsuda, M., Yachi, K., Hatori, N., Tanino, M., Kimura, T., Nishihara, H., Minami, A., Iwasaki, N., and Tanaka, S. (2014). SS18-SSX-regulated miR-17 promotes tumor growth of synovial sarcoma by inhibiting p21WAF1/CIP1. Cancer Sci. *105*, 1152–1159.

Nagai, M., Tanaka, S., Tsuda, M., Endo, S., Kato, H., Sonobe, H., Minami, A., Hiraga, H., Nishihara, H., Sawa, H., and Nagashima, K. (2001). Analysis of transforming activity of human synovial sarcoma-associated chimeric protein SYT-SSX1 bound to chromatin remodeling factor hBRM/hSNF2 alpha. Proc. Natl. Acad. Sci. U S A *98*, 3843–3848.

Nielsen, T.O., Poulin, N.M., and Ladanyi, M. (2015). Synovial sarcoma: recent discoveries as a roadmap to new avenues for therapy. Cancer Discov. *5*, 124–134.

Pacheco, M., and Nielsen, T.O. (2012). Histone deacetylase 1 and 2 in mesenchymal tumors. Mod. Pathol. *25*, 222–230.

Peng, C., Guo, W., Yang, Y., and Zhao, H. (2008). Downregulation of SS18-SSX1 expression by small interfering RNA inhibits growth and induces apoptosis in human synovial sarcoma cell line HS-SY-II in vitro. Eur. J. Cancer Prev. *17*, 392–398.

Pretto, D., Barco, R., Rivera, J., Neel, N., Gustavson, M.D., and Eid, J.E. (2006). The synovial sarcoma translocation protein SYT-SSX2 recruits beta-catenin to the nucleus and associates with it in an active complex. Oncogene *25*, 3661–3669.

Qi, C.F., Kim, Y.S., Xiang, S., Abdullaev, Z., Torrey, T.A., Janz, S., Kovalchuk, A.L., Sun, J., Chen, D., Cho, W.C., et al. (2012). Characterization of ARF-BP1/HUWE1 interactions with CTCF, MYC, ARF

and p53 in MYC-driven B cell neoplasms. Int. J. Mol. Sci. *13*, 6204–6219.

Saito, T., Nagai, M., and Ladanyi, M. (2006). SYT-SSX1 and SYT-SSX2 interfere with repression of E-cadherin by snail and slug: a potential mechanism for aberrant mesenchymal to epithelial transition in human synovial sarcoma. Cancer Res. *66*, 6919–6927.

Sanchez-Vega, F., Mina, M., Armenia, J., Chatila, W.K., Luna, A., La, K.C., Dimitriadoy, S., Liu, D.L., Kantheti, H.S., Saghafinia, S., et al. (2018). Oncogenic signaling pathways in the cancer genome Atlas. Cell *173*, 321–337.e10.

Shmueli, A., and Oren, M. (2005). Life, death, and ubiquitin: taming the mule. Cell *121*, 963–965.

Song, S.H., and Kim, T.Y. (2017). CTCF, cohesin, and chromatin in human cancer. Genomics Inform. *15*, 114–122.

Su, L., Cheng, H., Sampaio, A.V., Nielsen, T.O., and Underhill, T.M. (2010). EGR1 reactivation by histone deacetylase inhibitors promotes synovial sarcoma cell death through the PTEN tumor suppressor. Oncogene *29*, 4352–4361.

Su, L., Sampaio, A.V., Jones, K.B., Pacheco, M., Goytain, A., Lin, S., Poulin, N., Yi, L., Rossi, F.M., Kast, J., et al. (2012). Deconstruction of the SS18-SSX fusion oncoprotein complex: insights into disease etiology and therapeutics. Cancer Cell *21*, 333–347.

Trautmann, M., Sievers, E., Aretz, S., Kindler, D., Michels, S., Friedrichs, N., Renner, M., Kirfel, J., Steiner, S., Huss, S., et al. (2014). SS18-SSX fusion protein-induced Wnt/beta-catenin signaling is a therapeutic target in synovial sarcoma. Oncogene *33*, 5006–5016.

Udeshi, N.D., Svinkina, T., Mertins, P., Kuhn, E., Mani, D.R., Qiao, J.W., and Carr, S.A. (2013). Refined preparation and use of anti-diglycine remnant (K-epsilon-GG) antibody enables routine quantification of 10,000s of ubiquitination sites in single proteomics experiments. Mol. Cell Proteomics *12*, 825–831.

Verdin, E., and Ott, M. (2015). 50 years of protein acetylation: from gene regulation to epigenetics, metabolism and beyond. Nat. Rev. Mol. Cell Biol. *16*, 258–264.

Vlenterie, M., Hillebrandt-Roeffen, M.H., Schaars, E.W., Flucke, U.E., Fleuren, E.D., Navis, A.C., Leenders, W.P., Versleijen-Jonkers, Y.M., and van der Graaf, W.T. (2016). Targeting cyclin-dependent kinases in synovial sarcoma: palbociclib as a potential treatment for synovial sarcoma patients. Ann. Surg. Oncol. *23*, 2745–2752.

Wang, D., Kon, N., Lasso, G., Jiang, L., Leng, W., Zhu, W.G., Qin, J., Honig, B., and Gu, W. (2016). Acetylation-regulated interaction between p53 and SET reveals a widespread regulatory mode. Nature *538*, 118–122.

Wang, D., Kon, N., Tavana, O., and Gu, W. (2017). The "readers" of unacetylated p53 represent a new class of acidic domain proteins. Nucleus *8*, 360–369.

Wang, X., Taplick, J., Geva, N., and Oren, M. (2004). Inhibition of p53 degradation by Mdm2 acetylation. FEBS Lett. *561*, 195–201.

ISCI, Volume *13*

Supplemental Information

HDAC2 Regulates Site-Specific Acetylation of MDM2 and Its Ubiquitination Signaling in Tumor Suppression

Nikita Patel, Juehong Wang, Kumiko Shiozawa, Kevin B. Jones, Yanfeng Zhang, Jeremy W. Prokop, George G. Davenport, Naoe T. Nihira, Zhenyue Hao, Derek Wong, Laurel Brandsmeier, Sarah K. Meadows, Arthur V. Sampaio, Ryan Vander Werff, Makoto Endo, Mario R. Capecchi, Kelly M. McNagny, Tak W. Mak, Torsten O. Nielsen, T. Michael Underhill, Richard M. Myers, Tadashi Kondo, and Le Su

Transparent Methods

Cell culture and chemicals

Human synovial sarcoma cell lines SYO-1 (Akira Kawai, National Cancer Center, Tokyo, Japan) and Yamato-SS (Kazuyuki Itoh, Osaka Medical Center for Cancer and Cardiovascular Diseases, Japan) were cultured in RPMI-1640 and DMEM (Invitrogen) respectively, supplemented with 10% fetal bovine serum (FBS) (Invitrogen). Human embryonic kidney 293 (HEK293) cells were purchased from American Type Culture Collection (ATCC) and maintained in DMEM with 10% FBS. All cell lines were grown at 37°C, 95% humidity and 5% CO2.

All chemicals used in this study are commercially available: FK228 (Selleck Chemicals), SB939 (Abcam), PCI-24781 (Santa Cruz Biotechnology), Geneticin/G418 (Invitrogen), MG-132 (Santa Cruz Biotechnology), Cycloheximide (BioVision) and DMSO (Sigma-Aldrich).

To achieve stable knockdown of human MULE and p53 genes, SYO-1 cells were infected with control or MULE/p53-specific shRNA lentiviruses in regular growth medium, supplemented with 5 μg/ml Polybrene (Santa Cruz Biotechnology). Selection was carried out using Puromycin (Santa Cruz Biotechnology) (at the final concentration of 10μg/ml) to remove non-transduced cells. Resistant cells were then expanded and maintained in Puromycin-containing growth medium. The efficiency of knockdown was confirmed at the mRNA or protein levels. Control, MULE and p53 shRNA lentiviral particles were purchased from Santa Cruz Biotechnology.

To construct the 3×Flag tagging donor plasmid, we designed the dsDNA genomic blocks (IDT) corresponding to homolog arms of individual SSX2 isoform and sub-cloned them into the pFETCh plasmid. Cas9/gRNA oligos (IDT) were designed nearby the 3' stop codons of SSX2 and integrated into the PX330 plasmid. 2×10^6 cells were transfected with the two constructs (5μg each), using the Nucleofector Kit V (Lonza). After overnight incubation in regular medium, cells were

subjected to G418 selection at the concentration of 400 μg/ml for 7-10 days. Resistant cells were expanded in regular medium for downstream applications. The sequences of gRNAs and genomic blocks are listed below:

gRNAs and genomic blocks for SSX2A

gRNAs	
forward:	caccGACTGCGTGAGAGAAAACAGC
reverse:	aaacGCTGTTTTCTCTCACGCAGTC
Genomic blocks	
HOM1:	tccccgacctgcagcccagctAAGTGTAAATGGATTGTTTGTAACACAAGGATA AATGCTTGAGGATGGATACCCTATTTTCCATGATGTGATTATTACCCAT TGCATGCCTGTATCAAAGCATCTCATGTACCCCATAAGAATATACACC TGCTGCGTACCCACAAAATAAAGAACAAAAATTATTTTAAAACACTAA AAAACAATAAAATCAATTGCAGTAATAATATCAAAGCTCACCGATCACA GATCACTATAGCAGATATAATAATAATGGAAAAGTGTAAAATTGGTGAG AATTAAAAAAAAAAAATTGCAGCATCTGCGAAGCAGTATGAACATGAGG TGCAACAAAACAAGGTACGCCTGTGTGGCCTTAACAAATACGTGCTG GATGAAAGGAGGTATGGGGGAATGTTCCCGTAAGTGAAGAGGTTGG GAATCTAAGCCTGAGAAGGGAAGGAGCCAGAAGCTAAAACTTTAATT GGCATTTGGCCTATGTTGGTGTGGATCTAAGGTCTCAGCCTCTCTAA GCCAGAGAATGTGAAAAACTGGATGAAGAAGGCCCATGGGCACTTG GGAGGAAGCAGGCATCTCCTTTTTTTGAGTAAACAGAGCCTAACACT CTCCAACCTACCCAACCCTCACTTTCCAACTATTCTCCATCACAGGA CCCAAAAGGGGGGAACATGCCTGGACCCACAGACTGCGTGAGAGA AAAtAGtTGGgggagcggaggaggttccgg
HOM2:	agttcttctgattcgaacatcTTTATGAAGAGATCAGCGACCCTGAGGAAGATG ACGAGTAACTCCGTAAGAGAACCTTCCACTCATCCCCCACATCCCTG CAGACGTGCTATTCTGTTATGATACTGGTATCCCATCTGTCACTTGCT CCCCAAATCATTCCCTTCTTACAATTTTCTACTGTACAGCATTGAGGC TGAACGATGAGAGATTTCCCATGCTCTTTCTACTCCCTGCCCTGTATA TATCCGGGGATCCTCCCTACCCAGGATGCTGTGGGGTCCCAAACCC CAAGTAAGCCCTGATATGCGGGCCACACCTTTCTCTAGCCTAGGAAT TGATAACCCAGGCGAGGAAGTCACTGTGGCATGAACAGATGGTTCA CTTCGAGGAACCGTGGAAGGCGTGTGCAGGTCCTGAGATAGGGCA GAATCGGAGTGTGCAGGGTCTGCAGGTCAGGAGGAGTTGAGATTGC GTTGCCACGTGGTGGGAACTCACTGCCACTTATTTCCTTCTCTCTTC TTGCCTCAGCCTCAGGGATACGACACATGCCCATGATGAGAAGCAGA ACGTGGTGACCTTTCACGAACATGGGCATGGCTGCGGACCCCTCGT CATCAGGTGCATAGCAAGTGAAAGCAAGTGTTCACAACAGTGAAAAG TTGAGCGTCATTTTTCTTAGTGTGCCAAGAGTTCGATGTTAGCGTTTA CGTTGTATTTTCTTACACTcttggaaagtcctctccactg

gRNAs and genomic blocks for SSX2B

gRNAs	
forward:	caccGGATGTGGGGGATGAGTGGA
reverse:	aaacTCCACTCATCCCCCACATCC
Genomic blocks	
HOM1:	tccccgacctgcagcccagctTGAGGATGGATACCCTATTTTCCATGATGTGAT TATTACCCATTGCATGCCTGTATCAAAGCATCTCATGTACCCCATAAGA ATATACACCTGCTGCGTACCCACAAAATAAAGAACAAAAATTATTTTAA AACACTAAAAAACAATAAAATCAATTGCAGTAATAATATCAAAGCTCAC CGATCACAGATCACTATAGCAGATATAATAATAATGGAAAAGTGTAAAA TTGGTGAGAATTAAAAAAAAAAATTGCAGCATCTGCGAAGCAGTATGA ACATGAGGTGCAACAAAACAAGGTACGCCTGTGTGGCCTTAACAAAT ACGTGCTGGATGAAAGGAGGTATGGGGGAATGTTCCCGTAAGTGAA GAGGTTGGGAATCTAAGCCTGAGAAGGGAAGGAGCCAGAAGCTAAA ACTTTAATTGGCATTTGGCCTATGTTGGTGTGGATCTAAGGTCTCAGC CTCTCTAAGCCAGAGAATGTGAAAAACTGGATGAAGAAGGCCCATGG GCACTTGGGAGGAAGCAGGCATCTCCTTTTTTTGAGTAAACAGAGCC TAACACTCTCCAACCTACCCAACCCTCACTTTCCAACTATTCTCCATC ACAGGACCCAAAAGGGGGGAACATGCCTGGACCCACAGACTGCGT GAGAGAAAACAGCTGGTGATTTATGAAGAGATCAGCGACCCTGAGG AAGATGACGAGgggagcggaggaggttccgg
HOM2:	agttcttctgattcgaacatcACTCATCCCCCACATCCCTGCAGACGTGCTATTC TGTTATGATACTGGTATCCCATCTGTCACTTGCTCCCCAAATCATTCC CTTCTTACAATTTTCTACTGTACAGCATTGAGGCTGAACGATGAGAGA TTTCCCATGCTCTTTCTACTCCCTGCCCTGTATATATCCGGGGATCCT CCCTACCCAGGATGCTGTGGGGTCCCAAACCCCAAGTAAGCCCTGA TATGCGGGCCACACCTTTCTCTAGCCTAGGAATTGATAACCCAGGCG AGGAAGTCACTGTGGCATGAACAGATGGTTCACTTCGAGGAACCGT GGAAGGCGTGTGCAGGTCCTGAGATAGGGCAGAATCGGAGTGTGC AGGGTCTGCAGGTCAGGAGGAGTTGAGATTGCGTTGCCACGTGGT GGGAACTCACTGCCACTTATTTCCTTCTCTCTTCTTGCCTCAGCCTCA GGGATACGACACATGCCCATGATGAGAAGCAGAACGTGGTGACCTT TCACGAACATGGGCATGGCTGCGGACCCCTCGTCATCAGGTGCATA GCAAGTGAAAGCAAGTGTTCACAACAGTGAAAAGTTGAGCGTCATTT TTCTTAGTGTGCCAAGAGTTCGATGTTAGCGTTTACGTTGTATTTTCT TACACTGTGTCATTCTGTTAGATACTAACATTTTCATTGATGAGCAAGA CATACTTAATGCATATTcttggaaagtcctctccactg

Mouse work

All mouse experiments were approved by University of Utah and the University Health Network Committees on Animal Care. To generate mouse synovial sarcomas, the conditional SSM2 mice

were bred to Myf5-Cre mice, so as to express SS18-SSX2 in myoblasts and mesenchymal precursor cells (Haldar et al. 2007). The resulting Myf5-Cre/SSM2 progenies at age 14 weeks were subjected to weekly administration of FK228 or vehicle, and sacrificed at age 17 weeks for tumor collection. Tumor tissues were fixed in formalin and paraffin-embedded as standard pathology blocks. Blocks were serially sectioned at 6-μm thickness onto Fisher Plus microscope slides, prior to Hematoxylin and Eosin (H&E) staining. For immunofluorescence assay, slides were deparaffinized and rehydrated, prior to heat-induced antigen retrieval in Tris-EDTA buffer (pH=9). Non-specific staining was blocked by 10% goat serum in PBS for 60 min at room temperature, followed by incubation with human SSX2 antibody (BioSS Antibodies; 1:100 dilution in PBS with 10% goat serum) overnight at 4°C. After three PBS wash steps of 10 min, slides were incubated with the secondary goat anti-rabbit Alexa 594 antibody (Invitrogen) at 1:500 dilution for 30 min. After three PBS wash, slides were counterstained with DAPI (1:500 dilution) for 5 min, and mounted with Cytoseal-60 (Thermo Scientific). Microscopy analysis was taken with an Olympus BX-63 microscope and an Olympus XM-10 camera.

Mule-knockout mice, $Mule^{fl/+}$ (female) and $Mule^{fl/y}$ (male), were crossed to generate the E14.5 embryos for mouse embryonic fibroblast (MEF) isolation (Hao et al. 2012). $Mule^{fl/y}$ MEFs were transformed with pLPC-E1A-IRES-RasV12, before transduction with His-TAT-NLS-Cre, to induce Cre-based deletion of the floxed Mule allele. Loss of Mule expression was confirmed at the protein level by western blotting analysis.

Proximity ligation assay (PLA)

Cells were incubated on 8-well chamber slides (Sigma-Aldrich) overnight to 80% confluent. After 16-hr treatment with HDAC inhibitors, in the presence of MG-132 (1μM), cells were washed with

PBS, and fixed in 4% paraformaldehyde (PFA) (Santa Cruz Biotechnology) for 10 min at room temperature. Permeabilization was conducted with 0.5% Triton X-100 (in PBS) for 10 mins at room temperature. We used the Duolink kit (Sigma-Aldrich) for PLA experiments. Briefly, cells were blocked in Duolink Blocking Solution for 30 min at 37 °C, and incubated with primary antibodies (mouse anti-Flag, 0.5 μg/ml; rabbit anti-MULE, 1.0 μg/ml) for 90 min at room temperature, followed by 60-min incubation of the PLUS and MINUS probes at 37 °C. The probes were hybridized in the Duolink Ligation buffer for 30 min at 37°C, and PLA signals were strengthened by the amplification reaction (100 min at 37°C). Negative controls were set up with no primary antibodies. Slides were mounted using Duolink in situ mounting medium with DAPI and subjected to microscopy analysis.

Immunoprecipitation and western blots

Cell extracts were prepared using the RIPA Lysis Buffer system (Santa Cruz Biotechnology), and protein concentrations were measured by the Bradford protein assay (Bio-Rad). For immunoprecipitation, cell lysates were prepared using the Pierce IP Lysis Buffer (Thermo Scientific) with protease inhibitor cocktails (Roche). Equal amounts of cell lysates were incubated with Bio-Rad Protein-A/G magnetic beads (75 μl) coupled with primary antibodies (3-4 μg). After overnight rotation at 4°C, the beads were subjected to two washes with the IP buffer and two washes with PBS/T (0.1% Tween-20). Immunoprecipitates were eluted in 2× Laemmli buffer (10 min at 70°C). For western blot analysis, protein samples were separated on sodium dodecyl sulfate-polyacrylamide gel electrophoresis (SDS-PAGE), and transferred to 0.45 μm (or 0.2 μm) nitrocellulose membranes (Bio-Rad). Blots were incubated with the indicated primary antibodies (see below) and visualized using LI-COR Odyssey Infrared System.

List of primary antibodies used in this study

Abcam	
Histone H3:	Mouse monoclonal antibody (# ab10799)
MDM2 [SMP 14]:	Mouse monoclonal antibody (# ab3110)
Myc-tag [9E10]:	Mouse monoclonal antibody (# ab32)
Active Motif	
Histone H3ac (pan-acetyl):	Rabbit polyclonal antibody (# 61637)
Bethyl Laboratories	
Lasu1/Ureb1/MULE:	Rabbit polyclonal antibody (# A300-486A)
Bioss	
human SSX2/CT5.2:	Rabbit polyclonal antibody (# 11312R)
Cell Signaling Technology	
Acetylated-Lysine:	Rabbit polyclonal antibody (# 9814)
GeneTex	
GFP-tag:	Rabbit polyclonal antibody (# GTX113617)
MDM2:	Rabbit polyclonal antibody (# GTX100531)
SS18:	Rabbit polyclonal antibody (# GTX129428)
Millipore/Sigma	
CTCF:	Rabbit polyclonal antibody (# 07-729)
FLAG-tag (M2):	Mouse monoclonal antibody (# F1804)
α-Tubulin (DM1A):	Mouse monoclonal antibody (# T9026)
Santa Cruz Biotechnology	
β-Actin (C4):	Mouse monoclonal antibody (# sc-47778)
β-catenin (H-1):	Mouse monoclonal antibody (# sc-133240)
HDAC2 (3F3):	Mouse monoclonal antibody (# sc-81599)
HDAC3 (A-3):	Mouse monoclonal antibody (# sc-376957)
Mcl-1 (22):	Mouse monoclonal antibody (# sc-12756)
Ubiquitin (P4D1):	Mouse monoclonal antibody (# sc-8017)
Thermo Scientific	
HA-tag (2-2.2.14):	Mouse monoclonal antibody (# 26183)
HDAC1:	Rabbit polyclonal antibody (# PA1-860)
DYKDDDDK/FLAG-tag:	Rabbit polyclonal antibody (# 740001)

Protein structure modeling

Models for MULE (amino acids 2261-2970) were generated using I-TASSER hybrid modeler, and for MDM2 (amino acids 418-491) using YASARA homology modeling. Docking analysis was performed using the HADDOCK server, followed by energy minimization of each predicted interaction using both the AMBER03 and YASARA2 force fields. Evolutionary analysis and codon selection work was done using our published Sequence-to-Structure-to-Function methods (Prokop et al. 2017).

Ubiquitination analysis

For in vitro ubiquitination analysis, Myc-tagged SS18-SSX2 fusion protein was made by the TnT Quick Coupled Transcription/Translation system (Promega) and mixed with 35μg of either wild-type (WT) or Mule-null MEF cell extracts in the reaction buffer (50mM Tris-HCl, 10mM NaCl, 5mM $MgCl_2$, 1mM DTT, 20μM MG-132, 5mM ATP). After 60-min incubation at 30°C, samples were subjected to anti-Myc immunoprecipitation using antibody-coated magnetic beads (crosslinking with 20mM dimethyl pimelimidate/DMP, Sigma-Aldrich). Proteins in the eluent were separated on 8% SDS-PAGE, followed by western blotting against Myc and ubiquitin. For in vivo ubiquitination study, cells were treated with HDAC inhibitors for 12 hr, followed by adding 20μM MG-132 for 6 hr. The lysate was prepared using RIPA Lysis Buffer (Santa Cruz Biotechnology), sonicated by the Bioruptor (10 sec × 3 cycles, low power) and subjected to immunoprecipitation (primary antibody: 4μg/assay). Beads were washed twice with the RIPA buffer, followed by three PBS/T washes, and boiled in Bio-Rad sample buffer for SDS-PAGE and western blot analysis.

Mass spectrometry

The protein samples were separated by 12.5% SDS-PAGE and subjected to in-gel digestion using trypsin (Kondo and Hirohashi 2006). The tryptic digests were then subjected to liquid chromatography coupled with nanoelectrospray tandem mass spectrometry (Finnigan LTQ Orbitrap XL mass spectrometer; Thermo Fisher). The Mascot software package (version 2.5.1; Matrix Science) was used to search for the mass of each peptide ion peak against the SWISS-PROT database (Homo sapiens, 20205 sequences in the Swiss prot_2015_09.fasta file) using the following parameters – 3 or 4 missed cleavage; variable modifications: oxidation (Met) and acetylation (Lys); peptide tolerance: 10 p.p.m.; MS/MS tolerance: 0.8 Da; peptide charge: 2^+, 3^+ and 4^+.

Cell viability and colony formation assays

Human synovial sarcoma cells were cultured at 60% confluence, and transfected with indicated siRNAs using Lipofectamine RNAiMAX (Invitrogen). After 72 hours, cell cultures were incubated with the 3-(4,5-dimethylthiazol-2-yl)-2,5-diphenyltetrazolium bromide (MTT) solution (Sigma-Aldrich), and MTT formazan was solubilized in acidic isopropanol with 0.04N HCl. Absorbance was read at 570 and 630 nm with a colorimeter. Cell viability was calculated as the relative absorbance (570/630 nm), and normalized to control cells. To study drug effects, cell viability was examined at the 48-hr time point after treatment with HDAC inhibitors. For colony formation assay, control and MULE-deficient SYO-1 cells were grown to 80% confluence, and treated with HDAC inhibitors for 24 hours. Cells were seeded into 6-well plates at the density of 600 cells/well in regular growth medium, and cultured for 10 days with medium change every 2-3 days. Finally, cells were fixed with 10% formaldehyde for 30 min at room temperature and

stained with 0.5% crystal violet solution (20% methanol) for 10 min at room temperature. Plates were washed with water and air-dried overnight, prior to scanning.

RNA interference (RNAi)

Two individual small interfering RNAs (siRNAs) were purchased from Thermo Stealth RNAi collection, for MDM2 (HSS142909, HSS142911), HDAC1 (HSS104725, HSS104726), HDAC2 (HSS104728, HSS104729) and HDAC3 (HSS113050, HSS113051). At 60% confluence, cells were transfected with indicated siRNAs at the final concentration of 20 nM, using Lipofectamine RNAiMAX (Invitrogen) according to the manufacturer's instructions. For human SS18 (Santa Cruz Biotechnology) and SS18-SSX2 (sense: CAAGAAGCCAGCAGAGGAATT, antisense: UUCCUCUGCUGGCUUCUUGTT), RNAi reactions were carried out with 40-80 nM siRNAs. Knockdown efficiency was confirmed by western blots.

Plasmid DNA construction and transfection

Flag- and HA-tagged human MULE constructs have been used in previous studies (Zhang et al. 2011; Yi et al. 2015). SS18-SSX2 cDNA and deletion mutants (ΔSNH, ΔQPGY and ΔRD) were synthesized via Integrated DNA Technologies (IDT) and inserted into a Gateway pENTR1A vector. To make Myc-tagged SS18-SSX2, EcoR1-Not1 fragment was sub-cloned into the pcDNA4 mammalian expression vector (Invitrogen). To generate GFP-tagged fusions, pENTR1A constructs were subjected to Gateway recombination reactions, creating pcDNA-DEST47 (Invitrogen) expression clones. For lysine-to-arginine (KR) and -glutamine (KQ) substitution experiments, we used the Q5 Site-Directed Mutagenesis kit (New England Biolabs) with the PCR primers listed below. For overexpression, cells were transiently transfected with indicated plasmid

DNA using Lipofectamine 3000 reagent (Invitrogen). After 48 hours post transfection, cells were harvested for downstream applications.

The sequences of PCR primers used for site-directed mutagenesis

SS18-SSX2 constructs	
K13 - forward:	GAGGCAGCGAGGCAGGGGGGAGATCA
K13 - reverse:	GGGGCCGCGAAAGCCACAG
K23 - forward:	CTGCGATTCAGAGGATGTTGGATGAC
K23 - reverse:	CGGGAGTGATCTCCCCCT
K41/43 - forward:	AAGGACCTCAGAGTGTTCTCAG
K41/43 - reverse:	CCTCTATTCTGAGAGTCCATTATAC
MDM2 constructs	
5KR - forward:	agaaggaataggCCCTGCCCAGTATGTAGA
5KR - reverse:	ccttagcctcctTGCACATGTAAAGCAGGC
KR1 - forward:	aaaaggaataagCCCTGCCCAGTATGTAGA
KR1 - reverse:	ctttagcctcctTGCACATGTAAAGCAGGC
KR2 - forward:	agaaggaataagCCCTGCCCAGTATGTAGA
KR2 - reverse:	ccttagcttcttTGCACATGTAAAGCAGGC
KR3 - forward:	aaaaggaataggCCCTGCCCAGTATGTAGA
KR3 - reverse:	ctttagcttcttTGCACATGTAAAGCAGGC
KQ1 - forward:	aaaaggaataagCCCTGCCCAGTATGTAGA
KQ1 - reverse:	ctttagctgctgTGCACATGTAAAGCAGGC
KQ2 - forward:	caaaggaataagCCCTGCCCAGTATGTAGA
KQ2 - reverse:	ctgtagcttcttTGCACATGTAAAGCAGGC

Real-time qPCR and RNA-sequencing

Total RNA was isolated and then transcribed to cDNA using the Qiagen RNeasy kit and the high-capacity cDNA reverse transcription kit (Applied Biosystems), respectively. Taqman gene expression assays were performed on an ABI-7500 Fast Real-Time PCR System with human

MULE-specific primer/probe sets (Applied Biosystems). SS18-SSX2 fusion oncogene expression (5'-TGACCAGATCATGCCCAAG-3'; 5'-GGGTCCAGATCTCTCGTGAA-3') was measured by SYBR Green qPCR assay (Applied Biosystems). All transcript levels were normalized to expression of 18S ribosomal RNA (rRNA). For sequencing analysis, RNA isolated with RNAzol (Sigma-Aldrich) was quality-checked for the integrity scores greater than 8 on the Aligent Bioanalyzer, and then prepared and indexed with Truseq Stranded mRNA kit (Illumina). Sequencing was done on an Illumina HiSeq 2500 50 Paired End run. All data were aligned to hg19 using TopHat2, and differential expression was demonstrated through Cufflinks and normalized FPKM numbers.

Histone extraction

Cells were suspended at the density of 4×10^7 cells per ml in the solution (10mM HEPES, 10mM KCl, 1.5mM $MgCl_2$, 0.34M sucrose, 10% glycerol, 1mM DTT, 0.2% Triton X-100) and incubated for 5 min on ice. Nuclei were collected in pellet by low-speed centrifugation (4 min, 1,300×g, 4°C), washed once with PBS/T (0.5% Triton X-100) and resuspended in 0.2N HCl. After overnight incubation at 4°C, the supernatant was collected by high-speed centrifugation (10 min, 6,500×g, 4°C) and neutralized with 1M Tris-HCl (pH=8). Histone samples were separated on 15% SDS-PAGE and analyzed by coomassie blue staining (Protea SuperBlue) and western blotting.

Data and Software Availability

Original mass spectrometry files are deposited in the ProteomeXchange Consortium (the accession #PXD012540) and Japan Proteome Standard Repository/Database (#JPST000550). Raw data from RNA-sequencing are deposited in Gene Expression Omnibus (GEO) under #GSE126152.

Supplemental Figure Titles and Legends

Figure S1. HDAC inhibition reduces synovial sarcoma growth in a genetic mouse model of and downregulates SS18-SSX fusion oncoprotein in human synovial sarcoma cells, Related to Figure 1. (A) Outline of drug administration. (B) Total mass of tumors present at age 17 weeks in the thoracic cage of mice bearing the human SS18-SSX2 fusion oncogene induced by Myf5-Cre, after treatment with 3 weekly doses of FK228 or vehicle, beginning at age 14 weeks (mean of 5-8 samples per group ± SD). *, $P < 0.05$ by two-tailed Student's t-test. (C-H) Hematoxylin and eosin photomicrographs of tumors obtained from vehicle (C-E) or FK228 (F-H) treated mice demonstrating the normal synovial sarcoma morphology of control tumors, including monophasic (C) and biphasic (D) patterning, including frank gland formation (solid black arrows) that was not identified in any treated tumors, as well as infiltrative growth between muscle fibers (E). FK228-treated tumors had no glands remaining, and showed areas with inflammatory cells and hemosiderin laden macrophages (white arrows in F), areas where tumor cells were scant and collagen matrix was plentiful (G), and regions where apparent prior intramuscular infiltration was replaced with paucicellular fibrosis (open black arrows in H). All magnification bars are 50μm in length. (I) Outline of the CRISPR/Cas9 approach targeting the SSX2B gene. (J) Anti-Flag western blot analysis of fusion oncoprotein levels in parental and CRISPR cells expressing control or SS18-SSX2-specific siRNA. Actin serves as a loading control. (K) Immunoprecipitation of Flag-SS18-SSX2 from parental and CRISPR-modified SYO-1 cells. The lysates (Input) and mouse IgG serve as positive and negative controls, respectively. (L) Anti-Flag western blot analysis of SS18-SSX2 protein abundance in FK228-treated CRISPR cells at different time points. Tubulin was used as a loading control; parental cell lysate serves as a negative control. (M) RT-qPCR analysis of SS18-

SSX2 transcript levels in SYO-1 cells treated with HDAC inhibitors (FK228, SB939 and PCI-24781) at the 8- and 16-hour time points.

Figure S2. MULE does not interact with the SSX2A isoform in human synovial sarcoma cells, Related to Figure 3. (A) Amino-acid sequence comparison of the SSX2-A and -B isoforms. (B) Outline of the CRISPR/Cas9 approach targeting the SSX2A gene. (C) Western blot assay showing SSX2A protein (anti-Flag) immunoprecipitated from CRISPR-edited SYO-1 cells. Parental cells serve as a negative control. (D) Western blotting analysis of anti-Flag/-MULE immunoprecipitates from CRISPR cells treated with DMSO (–) or FK228 (30nM), in the presence of MG-132. Mouse IgG was used as a negative control. (E) Reciprocal immunoprecipitation showing no interaction between MULE and wild-type SS18 in HEK293 cells transfected with the plasmid encoding full-length MULE. Rabbit IgG serves as a negative control. (F) Western blot analysis of SS18 protein expression in wild-type and Mule-knockout MEF cells. Actin serves as a loading control.

Figure S3. Effect of MULE knockdown on histone acetylation and its known substrates upon HDAC inhibition, Related to Figure 4. (A) Schematic of a biochemical approach to isolate core histones. (B) Coomassie blue staining of total histone proteins isolated from indicated SYO-1 cell lines upon treatment of DMSO (–) or HDAC inhibitors (FK228 and SB939). (C) Under the same conditions, western blot analysis was performed to show the levels of total histone H3 and global histone H3 acetylation. (D) Western blot analysis of several known MULE substrates in response to HDAC inhibition (FK228 and SB939). Tubulin serves as a loading control. (E) Western blotting analysis showing the levels of CTCF, β-catenin and HDAC2 in control and MULE-knockdown SYO-1 cells treated with DMSO (–) or HDAC inhibitors. HDAC2 was used as a negative control

which stays constant upon HDAC inhibitor treatment, regardless of the MULE status. Tubulin and Actin serve as loading controls.

Figure S4. HDAC inhibition induces MULE upregulation through MDM2, Related to Figure 5. (A and B) Analysis of MULE mRNA (A) and protein (B) levels in SYO-1 and Yamato-SS cells treated with DMSO, FK228 or SB939. RT-qPCR data represent mean ± SD of three independent experiments; Tubulin was used as a loading control. (C) Anti-MULE western blot analysis of the lysate prepared from Yamato-SS cells treated with or without MG-132. Tubulin serves as a loading control. (D) Western blot analysis of anti-MULE immunoprecipitates from Yamato-SS cells in the presence of MG-132. Cell lysate (Input) and rabbit IgG serve as positive and negative controls, respectively. (E) Western blot analysis of the lysate from Yamato-SS cells transfected with control (–) or MDM2 siRNAs. Tubulin was used as a loading control. (F) Viability of Yamato-SS cells in response to MDM2 knockdown by two individual siRNAs. Values were normalized to control (–) knockdown; results represent mean ± SD of three independent experiments. (G) Western blotting of MDM2-knockdown SYO-1 cells stably expressing control or p53 shRNAs. Actin was used as a loading control. (H and I) Viability (H) and colony formation (I) assay of stable cell lines (as in G) in response to control or MDM2-specific siRNA transfection. Results represent mean ± SD of three independent experiments; representative image of colony formation assay shown in the right panel. (J) Ubiquitination analysis of endogenous MULE protein in vehicle (–), FK228- and SB939-treated Yamato-SS cells. Cell lysate (Input) was applied to show equal amounts of ubiquitin under all conditions. (K) Western blotting analysis of MULE protein abundance in DMSO- and FK228-treated Yamato-SS cells, upon exposure to cycloheximide (CHX) for the indicated time. Tubulin was used as a loading control. (L and M) Viability analysis of SYO-1 stable cell lines in response

to FK228 (L) and SB939 (M) at different concentrations. All results represent mean ± SD of three independent experiments. (N) Colony formation analysis of SYO-1 stable cell lines in response to FK228 and SB939 treatment. The image represents three independent experiments.

Figure S5. Effect of site-specific lysine acetylation on MDM2-MULE interaction in response to HDAC inhibition, Related to Figure 6. (A-E) Evolutionary and interaction data for MDM2 and MULE. (A) Predictions of 100 global HADDOCK docking for models of MDM2 (red) with MULE (gray). (B) Following one round of energy minimizations the using multiple force fields the top binding energy conformation was selected. Negatively charged amino acids are shown in red for MULE and positive charged residues in blue for MDM2. (C) Deep evolutionary analysis of MDM2 using open reading frame sequences of 180 species for codon alignment. Four species (mouse, human, zebrafish, and chicken) are highlighted to show the depth of vertebrate species used for the alignment. (D) Codon selection scores put on a 21-codon sliding window mapping functional domains and motifs of the MDM2 protein. (E) Zoomed view of MULE-interacting amino acids in the RING domain of MDM2, with scores for codon selection (dN-dS, rate of nonsynonymous variants minus rate of synonymous variants). (F) Alignment of the MDM2 KRD, showing highly conserved lysine residues across different species. (G) Schematic of wild-type and mutant MDM2 constructs with lysine-to-arginine substitution highlighted in red. (H) Western blot analysis of lysine acetylation in anti-HA immunoprecipitates from HEK293 cells expressing HA-MDM2 constructs (as in G) under the treatment of FK228. To calculate MDM2 acetylation levels, acetyl-lysine/total ratios of FK228-treated samples were first normalized to individual DMSO (–) controls, and then normalized to the wild-type (WT) level. All results represent the average of two independent experiments. (I) Western blot analysis of anti-HA immunoprecipitates from DMSO-

and FK228-treated HEK293 cells expressing HA-MDM2 (WT) or KR3, in the presence of MG-132. Input serves as loading control. (J) Band intensities of MULE-bound MDM2 were quantified by ImageJ and normalized to Input. Values of FK228-treated samples were further normalized to DMSO (−). Data represent mean ± SD of three independent experiments. (K) Western blot analysis of HEK293 cells expressing empty vector (−) or Flag-p53, along with the HA-MDM2 constructs. Actin was used as a loading control.

Figure S6. HDAC2, rather than HDAC1 and HDAC3, regulates MDM2-MULE association and SS18-SSX protein expression, Related to Figure 7. (A) Model proposing a role for HDAC enzyme(s) in stabilizing the MDM2-MULE complex through removal of acetylation signals. (B) Western blot analysis of anti-MDM2 immunoprecipitates from SYO-1 and Yamato-SS cells. The lysate (Input) and rabbit IgG serve as positive and negative controls, respectively. (C and D) Western blotting analysis of SYO-1 (C) and Yamato-SS (D) cell extracts showing the knockdown efficiency of HDAC1 and HDAC2 siRNAs. MDM2 protein levels remain constant in control and knockdown cells. Actin and Tubulin serve as loading controls. (E) Immunoprecipitation analysis of MDM2-MULE interaction in MG-132-treated Yamato-SS cells depleted of HDAC1 or HDAC2. Input and rabbit IgG serve as positive and negative controls, respectively. (F) RT-qPCR analysis of SS18-SSX2 transcript levels in SYO-1 cells expressing control (−) or HDAC2 siRNAs. Results represent mean ± SD of three independent experiments. (G) Western blot analysis of the lysate from control (−) and HDAC1-knockdown SYO-1 cells. Actin was used as a loading control. (H) Western blot assay showing the levels of SS18-SSX1 protein in Yamato-SS cells transfected with control (−), HDAC1 or HDAC2 siRNAs. Tubulin serves as a loading control. (I) Western blotting analysis of the lysate from SYO-1 (left) and Yamato-SS (right) cells depleted of HDAC3. Tubulin

serves as a loading control. (J and K) Nutlin-3a does not interfere with MDM2 association and downregulation of MULE in human synovial sarcoma cells. (J) Immunoprecipitation analysis of MDM2 binding to MULE in Nutlin-3a treated SYO-1 cells at the indicated concentrations, in the presence of MG-132. Rabbit IgG serves as a negative control. (K) Western blotting analysis of the lysate of SYO-1 cells treated with DMSO, Nutlin-3a (10μM) or FK228 (30nM). Tubulin was used as a loading control.

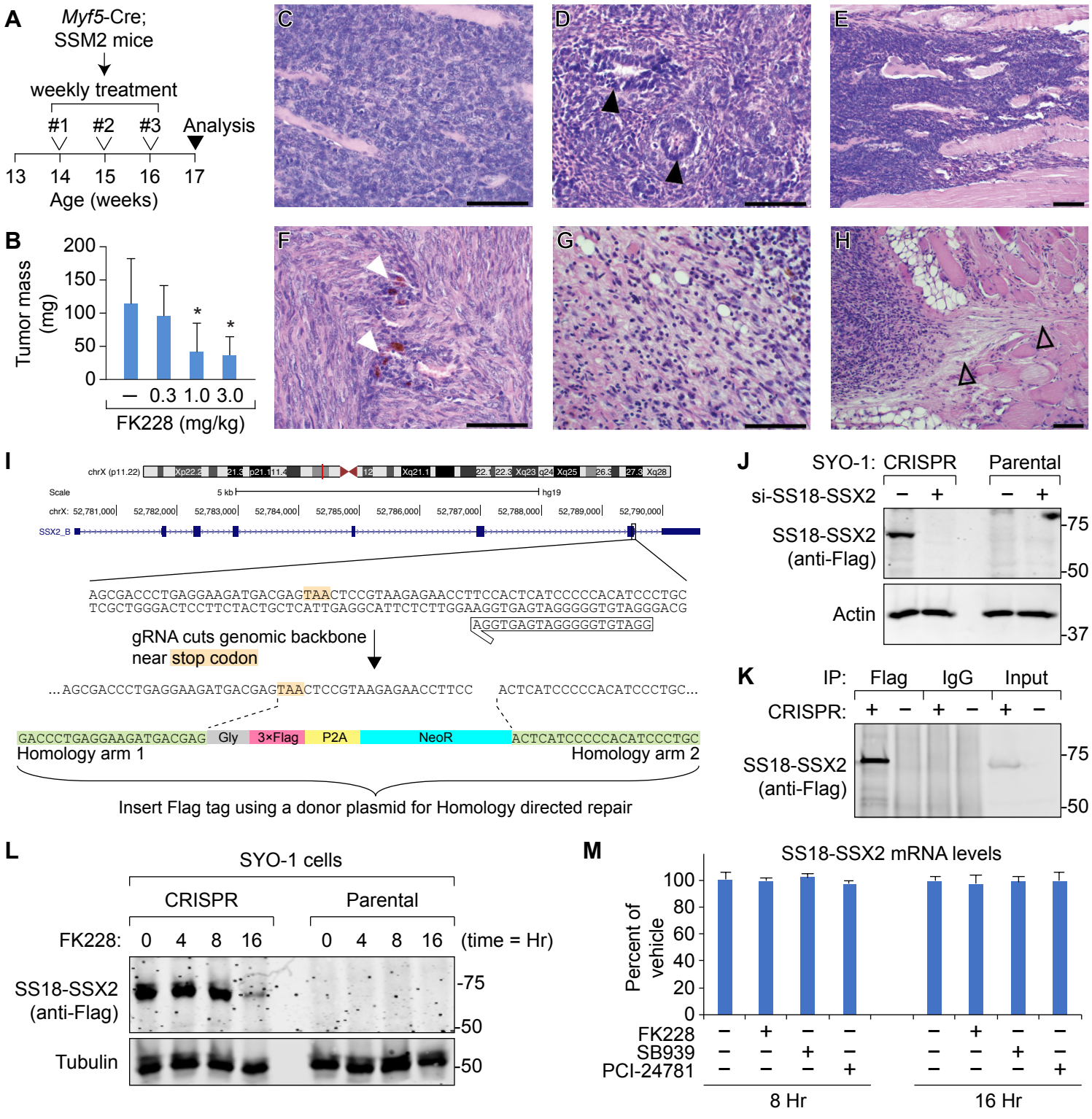
A
Myf5-Cre;
SSM2 mice
weekly treatment
#1 #2 #3 Analysis
13 14 15 16 17
Age (weeks)
B
Tumor mass (mg)
200
150
100
50
0
*
*
— 0.3 1.0 3.0
FK228 (mg/kg)
C
D
E
F
G
H
I
chrX (p11.22)
Scale
5 kb
hg19
chrX: 52,781,000 52,782,000 52,783,000 52,784,000 52,785,000 52,786,000 52,787,000 52,788,000 52,789,000 52,790,000
SSX2_B
AGCGACCCTGAGGAAGATGACGAGTAACTCCGTAAGAGAACCTTCCACTCATCCCCCACATCCCTGC
TCGCTGGGACTCCTTCTACTGCTCATTGAGGCATTCTCTTGGAAGGTGAGTAGGGGGTGTAGGGACG
AGGTGAGTAGGGGGTGTAGG
gRNA cuts genomic backbone
near stop codon
...AGCGACCCTGAGGAAGATGACGAGTAACTCCGTAAGAGAACCTTCC ACTCATCCCCCACATCCCTGC...
GACCCTGAGGAAGATGACGAG Gly 3×Flag P2A NeoR ACTCATCCCCCACATCCCTGC
Homology arm 1
Homology arm 2
Insert Flag tag using a donor plasmid for Homology directed repair
J
SYO-1: CRISPR Parental
si-SS18-SSX2 – + – +
SS18-SSX2
(anti-Flag)
75
50
Actin
37
K
IP: Flag IgG Input
CRISPR: + – + – + –
SS18-SSX2
(anti-Flag)
75
50
L
SYO-1 cells
CRISPR Parental
FK228: 0 4 8 16 0 4 8 16 (time = Hr)
SS18-SSX2
(anti-Flag)
75
50
Tubulin
50
M
SS18-SSX2 mRNA levels
Percent of vehicle
100
80
60
40
20
0
FK228 – + – – – + – –
SB939 – – + – – – + –
PCI-24781 – – – + – – – +
8 Hr
16 Hr

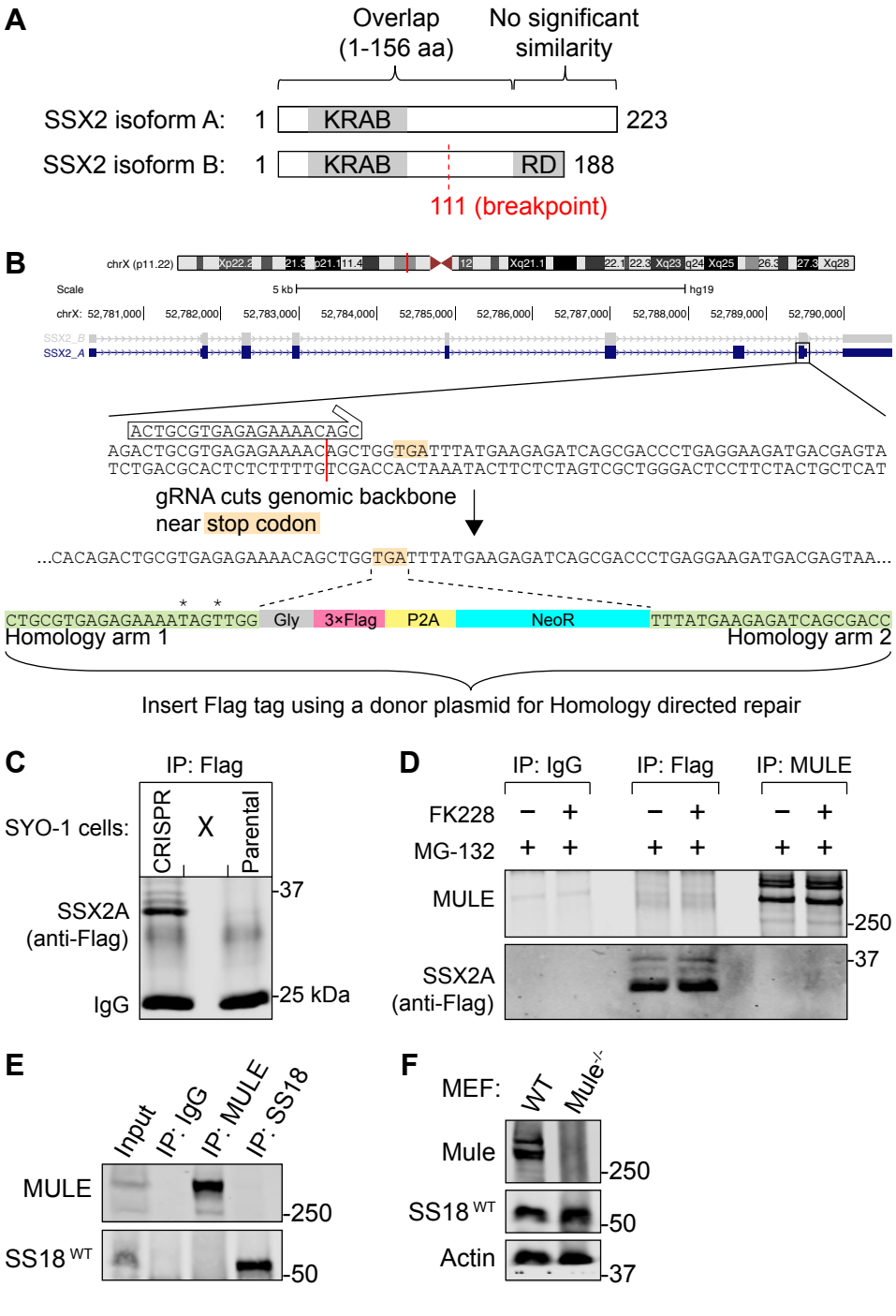
A
Overlap
(1-156 aa)
No significant
similarity
SSX2 isoform A: 1 KRAB 223
SSX2 isoform B: 1 KRAB RD 188
111 (breakpoint)
B
chrX (p11.22)
Scale
5 kb
hg19
chrX: 52,781,000 52,782,000 52,783,000 52,784,000 52,785,000 52,786,000 52,787,000 52,788,000 52,789,000 52,790,000
SSX2_B
SSX2_A
ACTGCGTGAGAGAAAACAGC
AGACTGCGTGAGAGAAAACAGCTGGTGATTTATGAAGAGATCAGCGACCCTGAGGAAGATGACGAGTA
TCTGACGCACTCTCTTTTGTCGACCACTAAATACTTCTCTAGTCGCTGGGACTCCTTCTACTGCTCAT
gRNA cuts genomic backbone
near stop codon
...CACAGACTGCGTGAGAGAAAACAGCTGGTGATTTATGAAGAGATCAGCGACCCTGAGGAAGATGACGAGTAA...
CTGCGTGAGAGAAAATAGTTGG Gly 3×Flag P2A NeoR TTTATGAAGAGATCAGCGACC
Homology arm 1
Homology arm 2
Insert Flag tag using a donor plasmid for Homology directed repair
C
IP: Flag
SYO-1 cells:
CRISPR
X
Parental
SSX2A
(anti-Flag)
IgG
37
25 kDa
D
IP: IgG
IP: Flag
IP: MULE
FK228 − + − + − +
MG-132 + + + + + +
MULE
SSX2A
(anti-Flag)
250
37
E
Input
IP: IgG
IP: MULE
IP: SS18
MULE
SS18 WT
250
50
F
MEF:
WT
Mule-/-
Mule
SS18 WT
Actin
250
50
37

Patel_Fig.S3

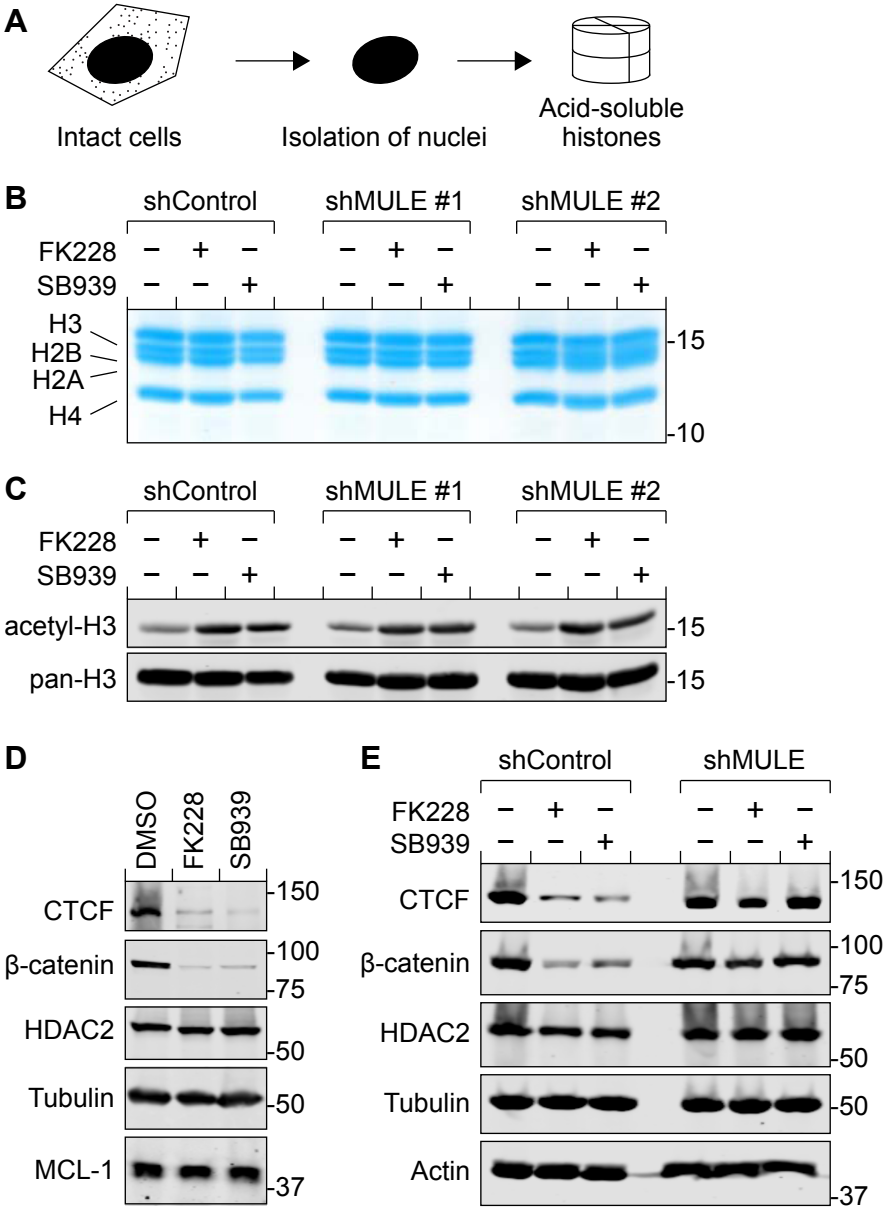
A
Intact cells
Isolation of nuclei
Acid-soluble histones
B
shControl
shMULE #1
shMULE #2
FK228
SB939
H3
H2B
H2A
H4
15
10
C
shControl
shMULE #1
shMULE #2
FK228
SB939
acetyl-H3
pan-H3
15
15
D
DMSO
FK228
SB939
CTCF
β-catenin
HDAC2
Tubulin
MCL-1
150
100
75
50
50
37
E
shControl
shMULE
FK228
SB939
CTCF
β-catenin
HDAC2
Tubulin
Actin
150
100
75
50
50
37

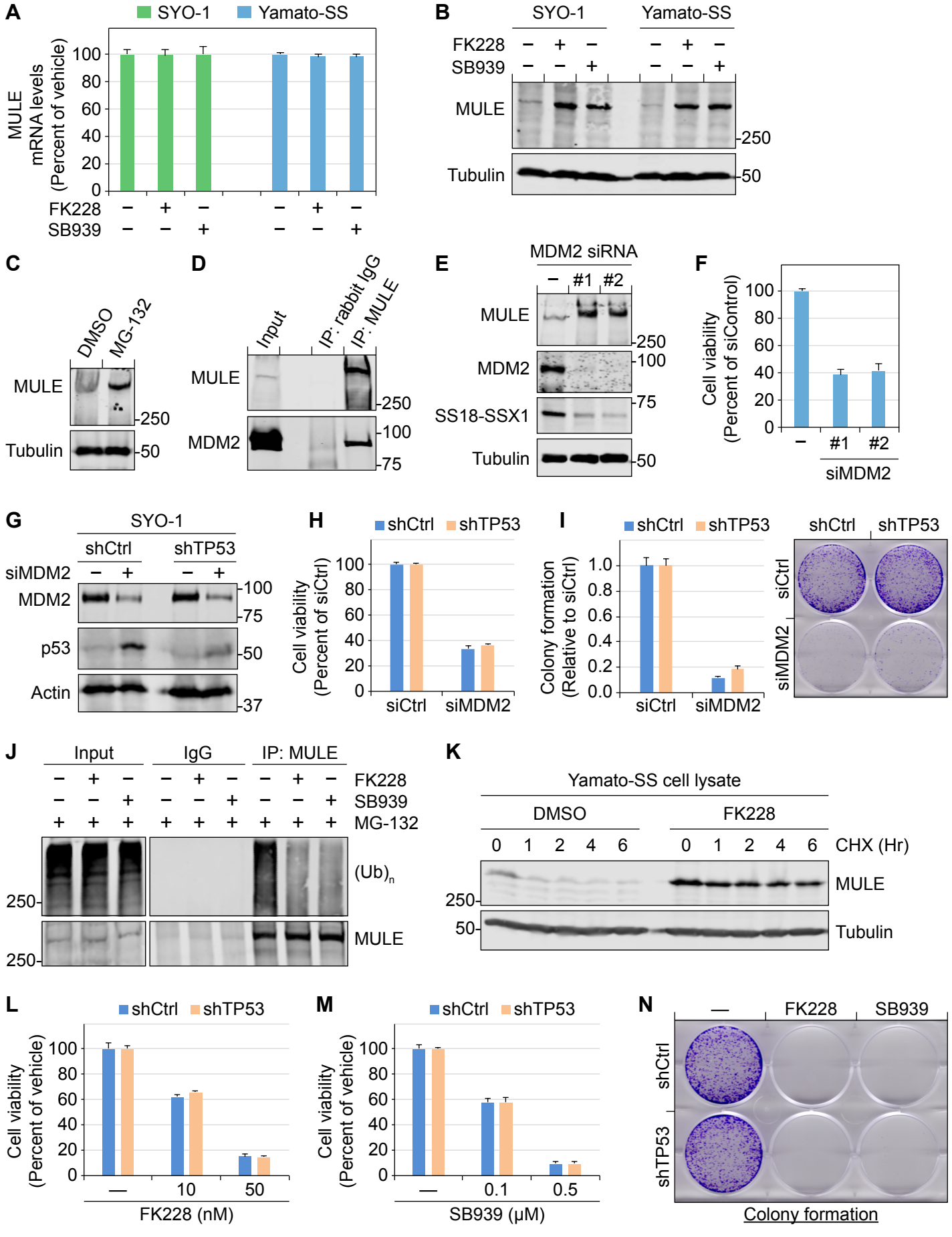
A
SYO-1
Yamato-SS
MULE mRNA levels (Percent of vehicle)
FK228
SB939
B
SYO-1
Yamato-SS
FK228
SB939
MULE
Tubulin
250
50
C
DMSO
MG-132
MULE
Tubulin
250
50
D
Input
IP: rabbit IgG
IP: MULE
MULE
MDM2
250
100
75
E
MDM2 siRNA
#1
#2
MULE
MDM2
SS18-SSX1
Tubulin
250
100
75
50
F
Cell viability (Percent of siControl)
siMDM2
G
SYO-1
shCtrl
shTP53
siMDM2
MDM2
p53
Actin
100
75
50
37
H
shCtrl
shTP53
Cell viability (Percent of siCtrl)
siCtrl
siMDM2
I
shCtrl
shTP53
Colony formation (Relative to siCtrl)
siCtrl
siMDM2
J
Input
IgG
IP: MULE
FK228
SB939
MG-132
(Ub)n
MULE
250
K
Yamato-SS cell lysate
DMSO
FK228
CHX (Hr)
MULE
Tubulin
250
50
L
shCtrl
shTP53
Cell viability (Percent of vehicle)
FK228 (nM)
M
shCtrl
shTP53
Cell viability (Percent of vehicle)
SB939 (μM)
N
FK228
SB939
shCtrl
shTP53
Colony formation

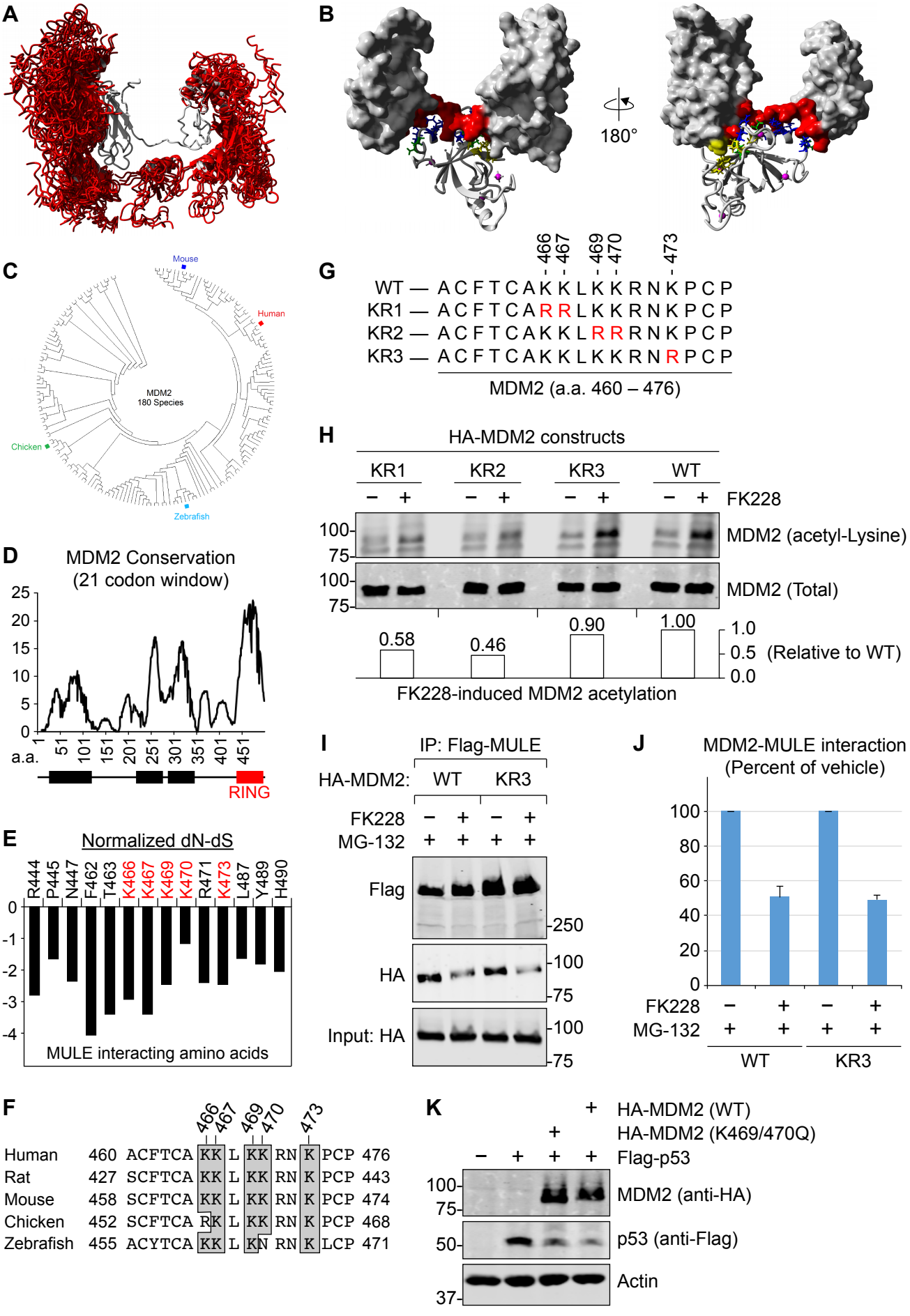
A
B
180°
C
Mouse
Human
MDM2
180 Species
Chicken
Zebrafish
D
MDM2 Conservation
(21 codon window)
a.a.
RING
E
Normalized dN-dS
R444 P445 N447 F462 T463 K466 K467 K469 K470 R471 K473 L487 Y489 H490
MULE interacting amino acids
F
466 467 469 470 473
Human 460 ACFTCA KK L KK RN K PCP 476
Rat 427 SCFTCA KK L KK RN K PCP 443
Mouse 458 SCFTCA KK L KK RN K PCP 474
Chicken 452 SCFTCA RK L KK RN K PCP 468
Zebrafish 455 ACYTCA KK L KN RN K LCP 471
G
466 467 469 470 473
WT — A C F T C A K K L K K R N K P C P
KR1 — A C F T C A R R L K K R N K P C P
KR2 — A C F T C A K K L R R R N K P C P
KR3 — A C F T C A K K L K K R N R P C P
MDM2 (a.a. 460 – 476)
H
HA-MDM2 constructs
KR1 KR2 KR3 WT
FK228
MDM2 (acetyl-Lysine)
MDM2 (Total)
0.58 0.46 0.90 1.00
(Relative to WT)
FK228-induced MDM2 acetylation
I
IP: Flag-MULE
HA-MDM2: WT KR3
FK228
MG-132
Flag
HA
Input: HA
J
MDM2-MULE interaction
(Percent of vehicle)
FK228
MG-132
WT KR3
K
HA-MDM2 (WT)
HA-MDM2 (K469/470Q)
Flag-p53
MDM2 (anti-HA)
p53 (anti-Flag)
Actin

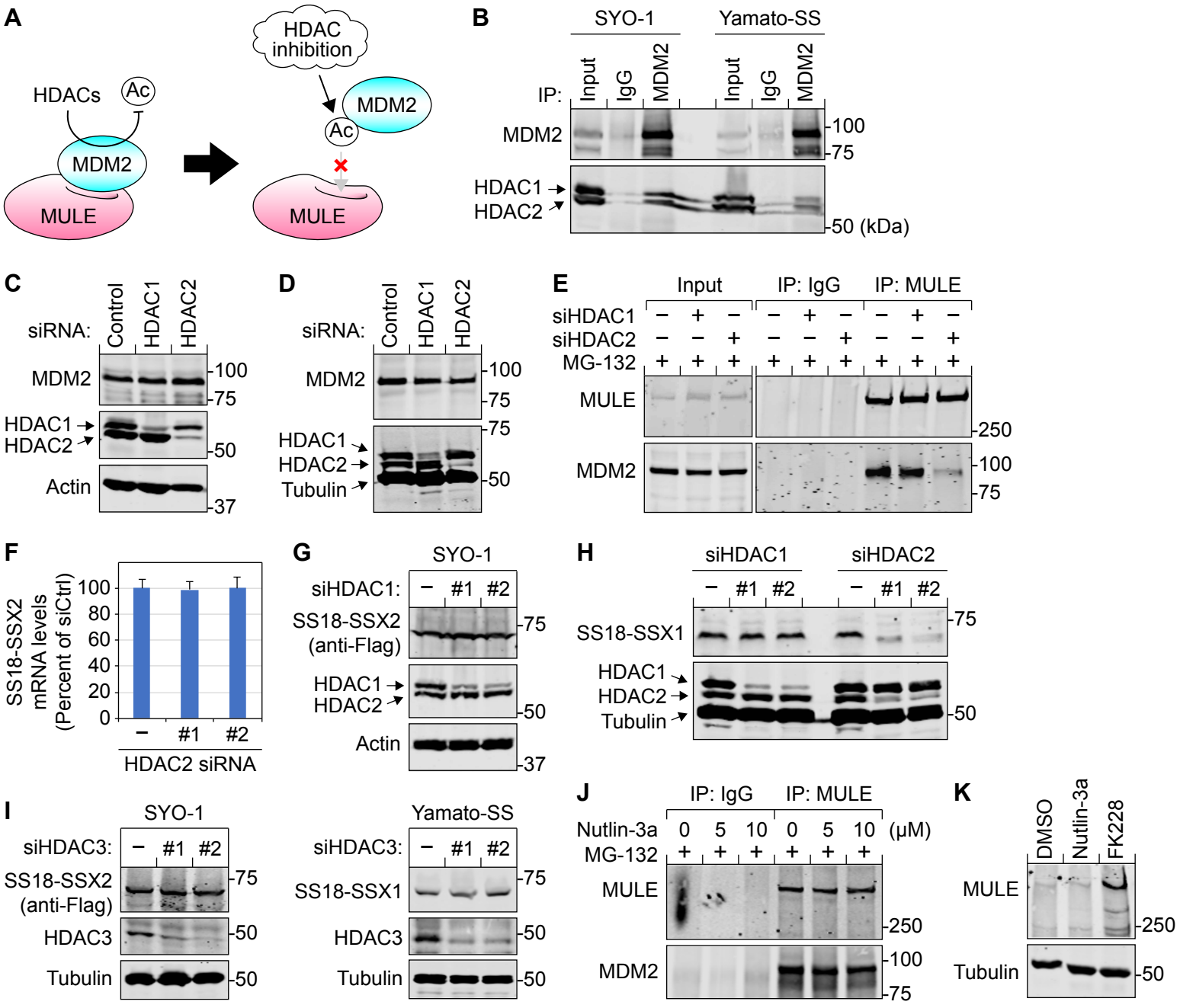
A
HDACs
Ac
MDM2
MULE
HDAC inhibition
MDM2
Ac
MULE
B
SYO-1
Yamato-SS
IP:
Input
IgG
MDM2
Input
IgG
MDM2
MDM2
HDAC1
HDAC2
100
75
50 (kDa)
C
siRNA:
Control
HDAC1
HDAC2
MDM2
HDAC1
HDAC2
Actin
100
75
50
37
D
siRNA:
Control
HDAC1
HDAC2
MDM2
HDAC1
HDAC2
Tubulin
100
75
75
50
E
Input
IP: IgG
IP: MULE
siHDAC1
siHDAC2
MG-132
MULE
MDM2
250
100
75
F
SS18-SSX2 mRNA levels (Percent of siCtrl)
100
80
60
40
20
0
–
#1
#2
HDAC2 siRNA
G
SYO-1
siHDAC1:
– #1 #2
SS18-SSX2 (anti-Flag)
HDAC1
HDAC2
Actin
75
50
37
H
siHDAC1
siHDAC2
– #1 #2 – #1 #2
SS18-SSX1
HDAC1
HDAC2
Tubulin
75
50
I
SYO-1
siHDAC3:
– #1 #2
SS18-SSX2 (anti-Flag)
HDAC3
Tubulin
75
50
50
Yamato-SS
siHDAC3:
– #1 #2
SS18-SSX1
HDAC3
Tubulin
75
50
50
J
IP: IgG
IP: MULE
Nutlin-3a
0 5 10 0 5 10 (μM)
MG-132
+ + + + + +
MULE
MDM2
250
100
75
K
DMSO
Nutlin-3a
FK228
MULE
Tubulin
250
50